# REPORT DOCUMENTATION PAGE

*Form Approved*

*OMB No. 0704-0188*



| 1. REPORT DATE *(DD-MM-YYYY)* | 2. REPORT TYPE | 3. DATES COVERED *(From - To)* |
|---|---|---|
| 08-01-2015 | Final | 28-Mar-2013 - 27-Sep-2015 |

**4. TITLE AND SUBTITLE**

Multi-Scale Porous Ultra High Temperature Ceramics

**5a. CONTRACT NUMBER**
FA2386-13-1-4068

**5b. GRANT NUMBER**
Grant AOARD-134068

**5c. PROGRAM ELEMENT NUMBER**
61102F

**6. AUTHOR(S)**

Dr. Carolina Tallon Galdeano

**5d. PROJECT NUMBER**

**5e. TASK NUMBER**

**5f. WORK UNIT NUMBER**

**7. PERFORMING ORGANIZATION NAME(S) AND ADDRESS(ES)**
University of Melbourne
Parkville, Vic
Parkville 3010
Australia

**8. PERFORMING ORGANIZATION REPORT NUMBER**
N/A

**9. SPONSORING/MONITORING AGENCY NAME(S) AND ADDRESS(ES)**

AOARD
UNIT 45002
APO AP 96338-5002

**10. SPONSOR/MONITOR'S ACRONYM(S)**
ADRL/AFOSR/IOA(AOARD)

**11. SPONSOR/MONITOR'S REPORT NUMBER(S)**
AOARD-134068

**12. DISTRIBUTION/AVAILABILITY STATEMENT**
Approved for public release.

**13. SUPPLEMENTARY NOTES**

**14. ABSTRACT**

This report summarizes the main outcomes of research to develop multi-scale porosity Ultra High Temperature Ceramic materials. Processing conditions were investigated and then optimized to prepare zirconium diboride ($ZrB_2$) and titanium diboride ($TiB_2$) porous materials with up to 92 % porosity by four different techniques: replica, particle stabilized foams, ice templating (freeze casting) and partial sintering. The pore morphology (closed-bubble-like porosity, open interconnected or lamellar porosity) and pore size (from 1 to 500 μm) can be fined tuned by optimizing the processing conditions. Selected conditions for each of these routes were used to explore the thermal conductivity and mechanical properties of the materials as a function of the porosity, pore size, shape and morphology. X-Ray Tomography was used to study their 3D microstructure. The 3D microstructures captured with tomography were used to produce virtual microstructures for prediction of the materials thermal and elastic properties. The Lattice Monte Carlo (LMC) approach was used to predict the materials thermal properties and Finite Element Analysis (FEA) used to predict the materials elastic properties. This modelling helped to understand the role of the porous material microstructural features such as the pore size, amount of porosity and pore shape. The approach can be extended to predict and evaluate the performance of these porous materials under extreme conditions, such as during hypersonic flights.

**15. SUBJECT TERMS**
Ultra High Temperature Ceramics, Colloidal Powder Processing, Multi-scale Porous Materials, Lattice Monte Carlo Method

| 16. SECURITY CLASSIFICATION OF: | | | 17. LIMITATION OF ABSTRACT | 18. NUMBER OF PAGES | 19a. NAME OF RESPONSIBLE PERSON |
|---|---|---|---|---|---|
| a. REPORT | b. ABSTRACT | c. THIS PAGE | | | Kenneth Caster, Ph.D. |
| U | U | U | SAR | 43 | 19b. TELEPHONE NUMBER *(Include area code)* +81-42-511-2000 |

# Report Documentation Page

*Form Approved*
*OMB No. 0704-0188*



| 1. REPORT DATE | 2. REPORT TYPE | 3. DATES COVERED |
|---|---|---|
| **08 JAN 2015** | **Final** | **28-03-2013 to 27-09-2014** |

| | |
|---|---|
| 4. TITLE AND SUBTITLE<br>**Multi-Scale Porous Ultra High Temperature Ceramics** | 5a. CONTRACT NUMBER<br>**FA2386-13-1-4068** |
| | 5b. GRANT NUMBER |
| | 5c. PROGRAM ELEMENT NUMBER<br>**61102F** |
| 6. AUTHOR(S)<br>**Carolina Tallon Galdeano** | 5d. PROJECT NUMBER |
| | 5e. TASK NUMBER |
| | 5f. WORK UNIT NUMBER |
| 7. PERFORMING ORGANIZATION NAME(S) AND ADDRESS(ES)<br>**University of Melbourne,Parkville, Vic,Parkville 3010,Australia,AU,3010** | 8. PERFORMING ORGANIZATION REPORT NUMBER<br>**N/A** |
| 9. SPONSORING/MONITORING AGENCY NAME(S) AND ADDRESS(ES)<br>**AOARD, UNIT 45002, APO, AP, 96338-5002** | 10. SPONSOR/MONITOR'S ACRONYM(S)<br>**AFRL/AFOSR/IOA(AOARD)** |
| | 11. SPONSOR/MONITOR'S REPORT NUMBER(S)<br>**AOARD-** |

12. DISTRIBUTION/AVAILABILITY STATEMENT
**Approved for public release; distribution unlimited**

13. SUPPLEMENTARY NOTES

14. ABSTRACT

**This report summarizes the main outcomes of research to develop multi-scale porosity Ultra High Temperature Ceramic materials. Processing conditions were investigated and then optimized to prepare zirconium diboride (ZrB2) and titanium diboride (TiB2) porous materials with up to 92 % porosity by four different techniques: replica, particle stabilized foams, ice templating (freeze casting) and partial sintering. The pore morphology (closed-bubble-like porosity, open interconnected or lamellar porosity) and pore size (from 1 to 500 m) can be fined tuned by optimizing the processing conditions. Selected conditions for each of these routes were used to explore the thermal conductivity and mechanical properties of the materials as a function of the porosity, pore size, shape and morphology. X-Ray Tomography was used to study their 3D microstructure. The 3D microstructures captured with tomography were used to produce virtual microstructures for prediction of the materials thermal and elastic properties. The Lattice Monte Carlo (LMC) approach was used to predict the materials thermal properties and Finite Element Analysis (FEA) used to predict the materials elastic properties. This modelling helped to understand the role of the porous material microstructural features such as the pore size, amount of porosity and pore shape. The approach can be extended to predict and evaluate the performance of these porous materials under extreme conditions, such as during hypersonic flights.**

15. SUBJECT TERMS
**Ultra High Temperature Ceramics, Colloidal Powder Processing, Multi-scale Porous Materials, Lattice Monte Carlo Method**

| 16. SECURITY CLASSIFICATION OF: | | | 17. LIMITATION OF ABSTRACT | 18. NUMBER OF PAGES | 19a. NAME OF RESPONSIBLE PERSON |
|---|---|---|---|---|---|
| a. REPORT<br>**unclassified** | b. ABSTRACT<br>**unclassified** | c. THIS PAGE<br>**unclassified** | **Same as Report (SAR)** | **43** | |

**Standard Form 298 (Rev. 8-98)**
Prescribed by ANSI Std Z39-18

# MULTI-SCALE POROUS ULTRA HIGH TEMPERATURE CERAMICS

**Dr. Carolina Tallon[1,2] and Prof. George V. Franks[1,2]**

[1]*Department of Chemical and Biomolecular Engineering, The University of Melbourne, VIC, Australia*
[2]*Defence Materials Technology Centre (DMTC), VIC, Australia*

## Final Report

Grant Number: FA2386-13-1-4068
Project Manager: Dr. Ken Caster
Period of performance: 27 March 2014-27 September 2014

## 0. Executive Summary

This report summarizes the main outcomes of our research funded by the AOARD to develop multi-scale porosity Ultra High Temperature Ceramic materials. We have optimized the processing conditions to prepare zirconium diboride ($ZrB_2$) and titanium diboride ($TiB_2$) porous materials with up to 92 % porosity by four different techniques: replica, particle stabilized foams, ice templating (freeze casting) and partial sintering. The pore morphology (closed-bubble-like porosity, open interconnected or lamellar porosity) and pore size (from 1 to 500 um) can be fined tuned by optimizing the processing conditions. Selected conditions for each of these routes were used to explore the thermal conductivity and mechanical properties of the materials as a function of the porosity, pore size, shape and morphology. X-Ray Tomography was used to study their 3D microstructure. These 3D microstructure captured with the tomography was used to produce virtual microstructures for prediction of the materials thermal and elastic properties. The Lattice Monte Carlo (LMC) approach was used to predict the materials thermal properties and the Finite Element Analysis (FEA) was used to predict the materials elastic properties. The modelling helped to understand the role of the porous material microstructural features such as the pore size, amount of porosity and pore shape. The approach can be extended to predict and evaluate the performance of these porous materials under extreme conditions, such as during hypersonic flights.

**Outline**

## 1. Motivation

The effort to produce a vehicle able to sustain flight under hypersonic conditions require the best matching between aerodynamic design and materials selection for such extreme conditions. Ultra High Temperature Ceramics (UHTCs) have been selected as the most promising candidate materials to be used in the parts of the vehicle where the heat load would reach temperatures closer to 3000$^{o}$C, such as leading edges and combustor (1).

The integration of these "*hot zones*" to the rest of the airframe is also paramount for a successful flight. It involves the development of innovative thermal protective systems to manage that heat load without compromising the weight of the vehicle. One of those options would be the utilization of an insulation package. The insulation package must be lightweight, high thermal and oxidation resistance, have a suitable mechanical integrity, low thermal conductivity and be able to accommodate a complex geometry during the integration (2).

Traditionally, the insulation packages are made out of ceramic oxides or carbon (1); however these materials are not suitable for ultra high temperature ceramics and are not very oxidation resistance. An insulation package made out of UHTCs would be the ideal solution to this problem, not only because of the temperature and oxidation resistance, but also to accommodate better the integration with the heat zones minimizing the mismatching of thermal expansion coefficient between the leading edges or combustor and the insulation.

The objective of this project is to develop highly porous UHTC materials which have the potential to be used in insulation packages for ultra high temperature applications, such as hypersonic flights. In order to manage the expected thermal flux, the material would feature a multi-scale porosity that would accommodate and allow for better control of the heat transfer. The routes proposed to manufacture such materials rely on the combination of colloidal processing techniques and pressureless sintering (3-6). Colloidal processing enables the control of the interparticle forces of UHTC particle in suspension to minimize defects and flaws while enhancing the particle packing in the shaped body, which lead to successful densification under pressureless conditions. Colloidal processing techniques also provide many options to produce different amounts of porosity as well as different pore shapes and sizes, as desired in this project. And finally, the colloidal processing and presssureless sintering combination will allow for the preparation of complex-shaped-geometry porous materials for easier integration in the vehicle.

The selected materials for this work are zirconium diboride ($ZrB_2$) and titanium diboride ($TiB_2$). $ZrB_2$ was chosen since it is a reference material in the UHTC community and it is well known and characterized, and because its excellent oxidation resistance. $TiB_2$ was also selected for this work

since it is one of the UHTC with lower densities and could produce an even more lightweight component. However, it was also chosen to study and test the versatility of the processing techniques to accommodate different materials, since it is likely that the final insulation package would comprise a mixture of different UHTC materials.

The processing techniques useful to produce porous ceramics (7-8) to be used in the research are the following:

- Replica
- Particle stabilized foams
- Ice templating (freeze casting)
- Partial sintering

Although there are other more "outside-of-the-box" innovative techniques to create porous materials, the techniques above have been selected because of their ability to produce near-net-shapes with complex geometries and large sizes while avoiding drying cracking in ceramics. The multi-scale porosity will be created by combining these techniques in a number of ways in the same material to target the desired thermal conductivity.

The thermal and mechanical behaviour of the porous ceramics will be modelled in order to predict their behaviour under operating conditions using the dense material properties and the material microstructure. The material microstructure will be captured using x-ray computed tomography. A virtual microstructure will be constructed from the 2D X-ray tomography slices and used to model the porous material properties. The 3D reconstruction will be meshed in order to complete the modelling. The thermal properties will be modelled using the Lattice Monte Carlo (LMC) simulation method. Mechanical properties will be modelled using Finite Element Analysis (FEA).

## 2. Processing Conditions Optimization

In this section, we present a summary of the different methods used to produce porous materials. We include the steps of the process, which parameters were optimized and studied, how the samples were characterized and the preliminary results for each of the selected techniques. (*The complete detailed study will be provided in the manuscripts under preparation).*

### 2.1. Replica

*a) Steps of the Process.*

In the replica technique, a polymeric sponge is used as a template to create the porous structure (7-8). The sponge is dipped into the stabilized well dispersed suspension until it has been fully coated (Figure 1). The sample is carefully dried. The green body containing the polymeric sponge is then sintered. The sponge is calcined in the earlier stages of the sintering (lower heating rates and dwell times around 400C), leaving a porous structure behind which resemble the porous structure of the polymeric sponge.

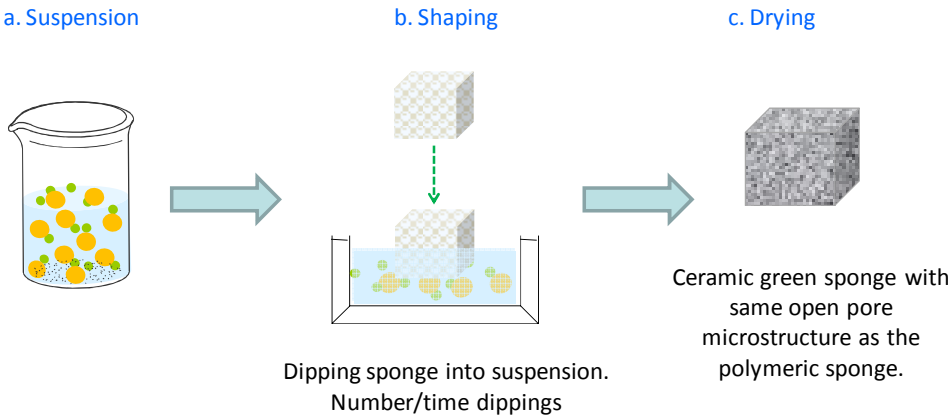


**Figure 1. Steps of the replica process**

*b) Parameters studied and optimized.*

- Solid content of the suspension
- Amount of dispersant with respect to powder
- Dipping time (time the sponge is immersed into the suspension)
- Number of dippings.
- Sintering temperature under vacuum.

*c) Characterization.*

- Rheology of suspensions
- Density and porosity
- Scanning Electron Microscopy (SEM)

*d) Results (see Figures 2 and 3)*

- Open and interconnected porous structures
- Macroporosity in the 400-1000 um range
- Overall porosity between 50 and 95%
- Strong enough to be handled and slightly machined in green and sintered states.
- No significant change of porosity/pore size after sintering
- Densification of particles in the struts
- Different templates can be used to produce different microstructures.

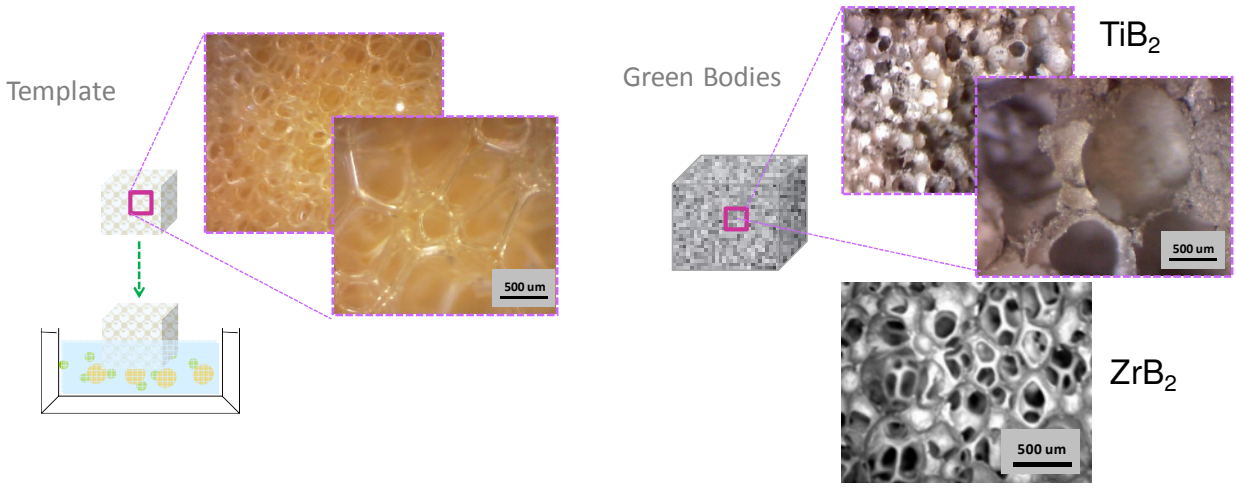


**Figure 2. Micrographs of the template sponge and the $TiB_2$ and $ZrB_2$ produced by the replica technique.**

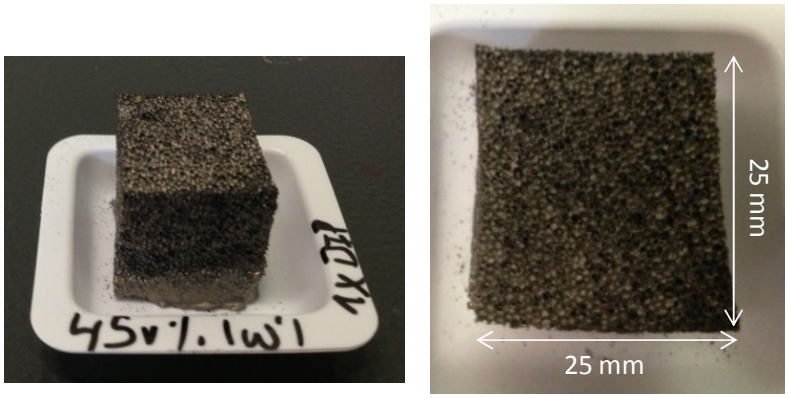


**Figure 3. Replica samples produced in this study.**

## 2.2. Particle Stabilized Foams

*a) Steps of the process*

Porous materials are created by the combination of the particle stabilized foam (8-12) and gelcasting concepts (5-6). The process steps are shown in Figure 4. The ceramic particles in the suspension are made weakly hydrophobic by the addition of a surfactant, which adsorbs at the particles surfaces. The ceramic suspension is formulated with the polymer (PVA) and crosslinking agent (DHF) required for the later gelcasting. (13) After homogenization and equilibrium, air bubbles are incorporated into the suspension by whipping. The weakly hydrophobic particles sit at the water-air interface, decorating the air bubbles and stabilizing the foam. The gelcasting reaction is then triggered, to lock the particles and bubbles in place and to allow for casting into the desired geometry.

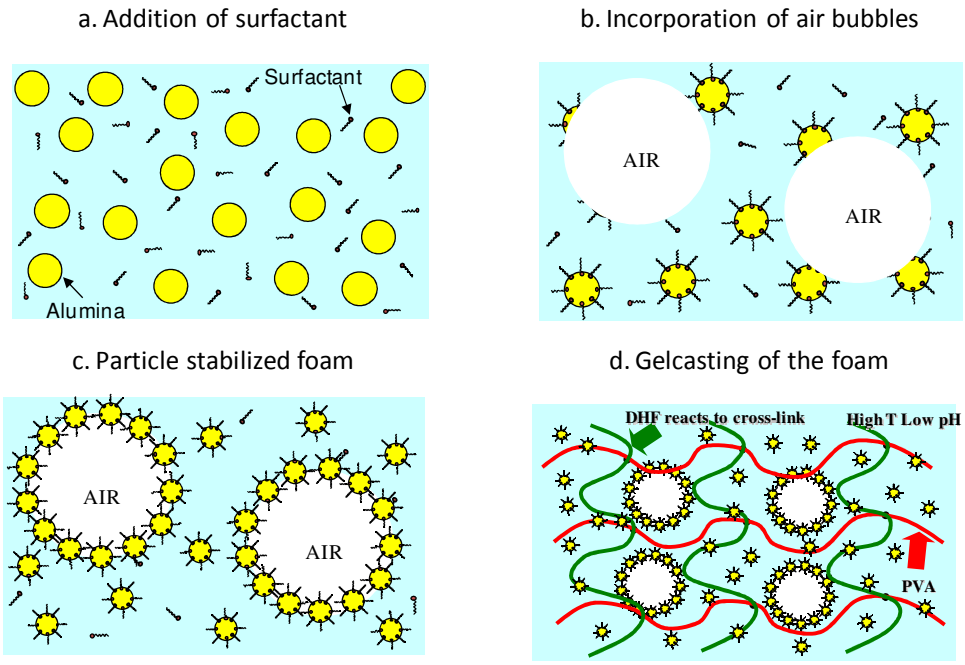


**Figure 4. Schematic illustration of the steps in the particle stabilized foams and gelcasting process.**

*b) Parameters optimized*

- Solid content of the suspension
- Amount of PVA with respect to solution
- Surfactant addition or not; surfactant amount.
- Aeration time (amount of air introduced into the suspension by whipping the suspension using a kitchen mixer). (See Figures 5 and 6)
- Sintering temperature under vacuum.


**Figure 5. Images of the foaming of the suspension**

*c) Characterization*

- Zeta Potential of particles.
- Rheology of suspensions.
- Densities and porosities
- Pore size
- Scanning electron microscopy (SEM)

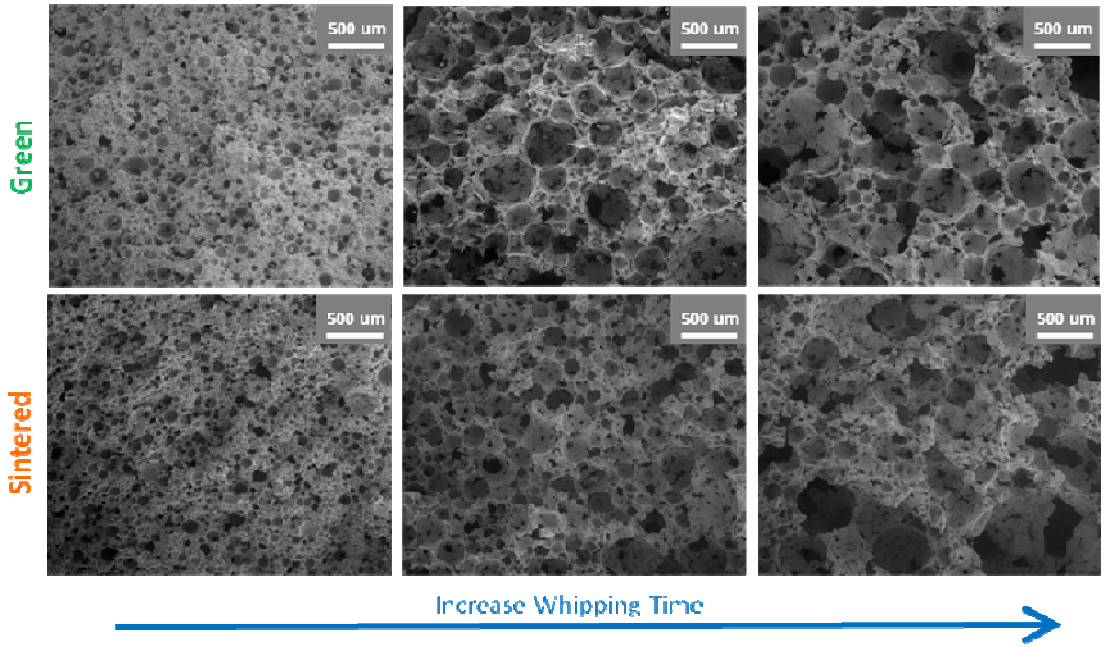


**Figure 6. Effect of the aeration time (whipping time) on the green and sintered $TiB_2$ foams.**

*d) Results*

- Closed-Bubble-like porosity
- Porosities and pore sizes:

  $TiB_2$: 70-93% porosity; Pore size: 80-200 um

  $ZrB_2$: 60-89% porosity; Pore size : to be measured
- No significant reduction of porosity/pore size upon sintering.
- Densification of the particles in the struts.
- Differences in Surface Chemistry: PVA role in the foam processing: surface agent/flocculant vs gelcasting additive. $TiB_2$ is hydrophobic enough to stabilize air bubbles without the need of surfactant. $ZrB_2$ is not hydrophobic enough to stabilize air bubbles. Surfactant addition is needed (See Figure 7).

**a)** **b)**

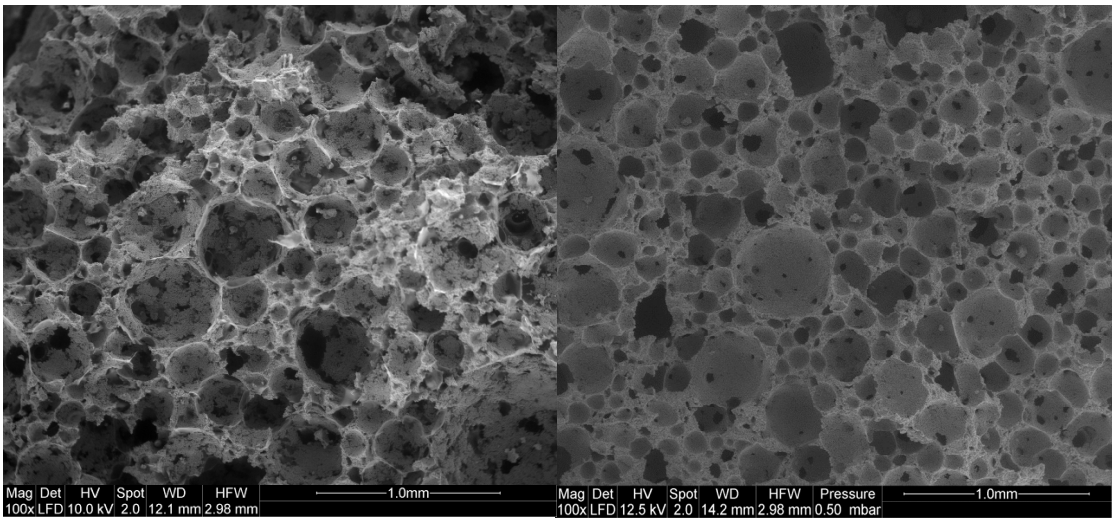


**Figure 7. a) $TiB_2$ foam prepared with no surfactant; b) $ZrB_2$ foam prepared with surfactant**

## 2.3. Ice Templating

*a) Steps of the process*

The pores are created by ice crystals which form during freezing of the suspension pushing the particles into the space between crystals. The size and shape of the porosity can be controlled by the suspension formulation and freezing condition. The ceramic suspension is poured into the mold. The mold is frozen according to the desired conditions. The frozen solvent ice crystals produce the porous structure. Once the sample is frozen, it is unmolded and freeze-dried. The frozen solvent is sublimated under vacuum leaving a porous structure (3, 14). The sublimative freeze drying also

minimised drying cracking. The green sample is then sintered into a consolidated porous structure as shown in Figure 8.

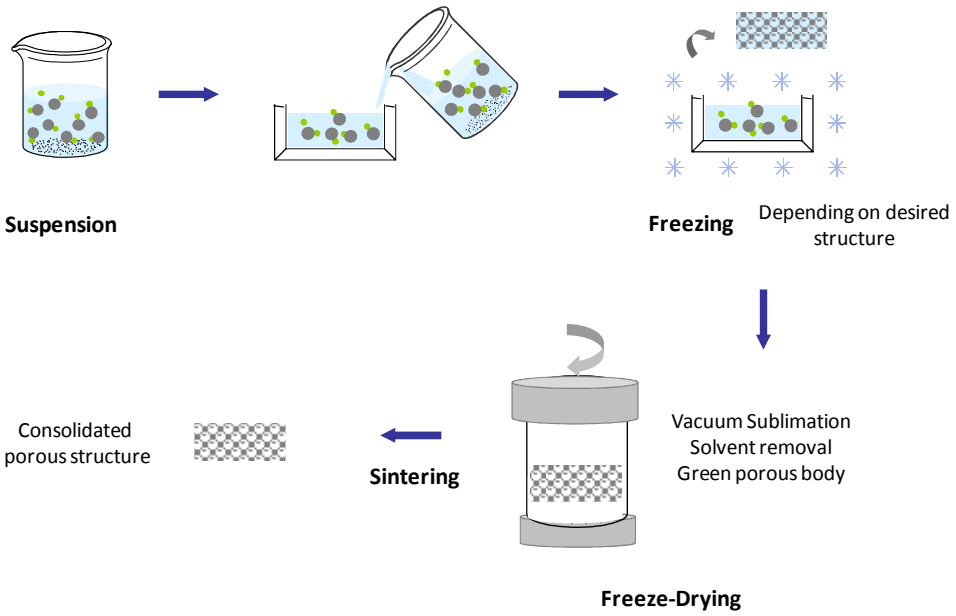


**Figure 8. Steps of the ice templating process**

*b) Parameters studied and optimized*

- Solid content of the suspension
- Solvent type: Aqueous vs non-aqueous
- Binder addition
- Freezing Temperature (and freezing rate)
- Sintering temperature under vacuum

*c) Characterization*

- Rheology of suspensions
- Densities and porosities
- Scanning Electron Microscopy

*d) Results*

- Combination of open and interconnected with closed porosity
- Porosity and pore size: 50-93% porosity; Pore size: 80-200 um
- No significant reduction of porosity/pore size upon sintering
- Densification of the particles in the struts

- Differences in morphology due to freezing conditions (See Figure 9): Binder addition influences ice structure; lamellar structure was found when water is used as solvent at low temperature; Directional Freezing; change of microstructure with change of solvent.

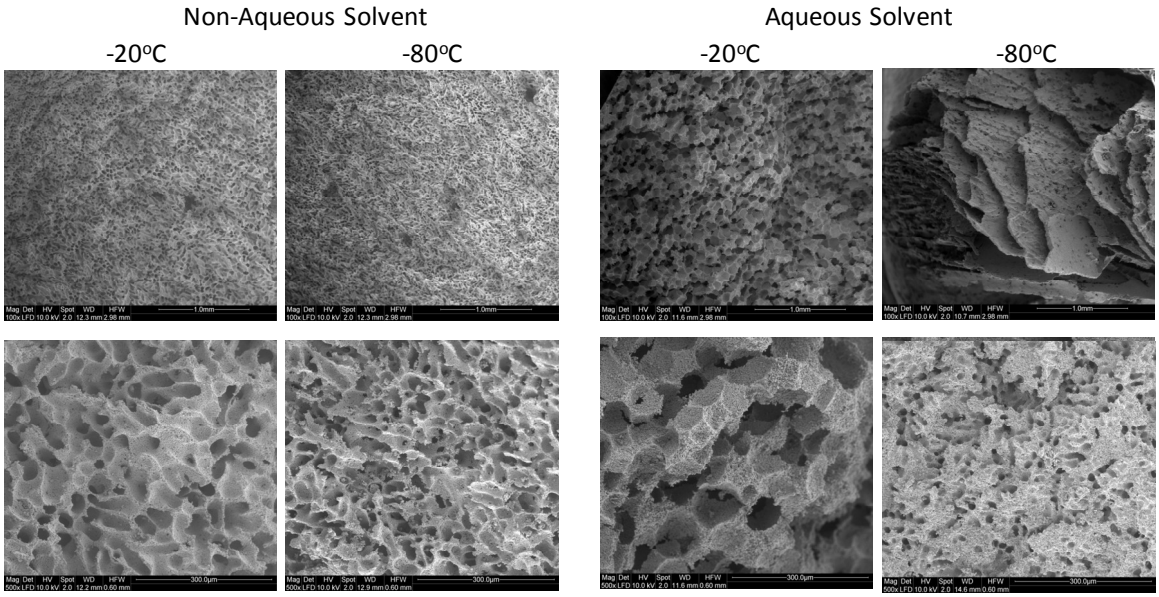


**Figure 9. Change of pore morphology under different porous conditions**

## 2.4. Partial Sintering

*a) Steps of the process*

The samples produced by any of the other techniques can be sintered at different temperatures. The sintering temperature is chosen to avoid full densification of the particles in the struts. Instead, sintering only to the necking stage results in strengthening the particle network but leaving the porosity in the "space" between the particles in the struts. The sintering temperature is selected to allow for particle necking and webbing extensively enough to provide good mechanical strength.

*b) Parameters optimized*

- Sintering temperature
- Solid content of the suspension

*c) Characterization*

- Densities and porosities
- Scanning electron microscopy (SEM)

*d) Results*

- Additional 10-20% Meso/Microporosity when sintering materials produced by any of the other processing techniques described.
- Micron-to-submicron pore sizes (See Figure 10).

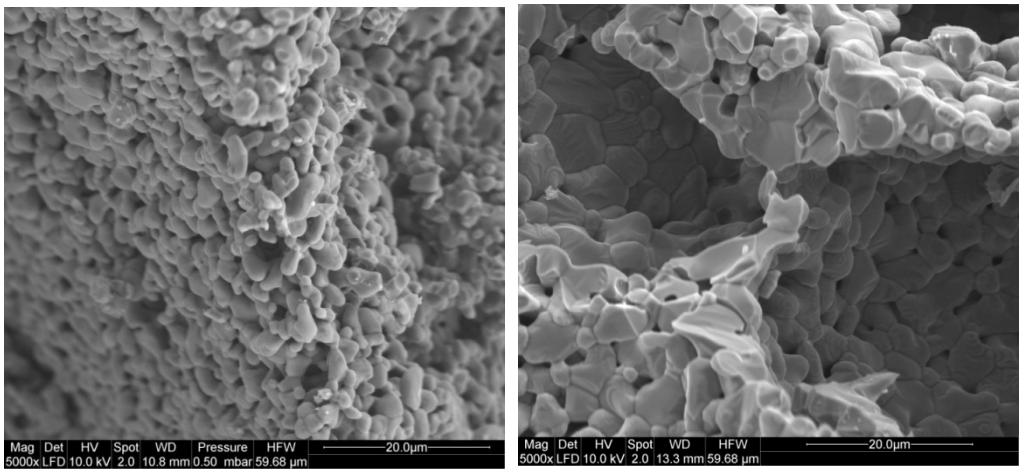


**Figure 10. SEM images of partially sintered samples 2000 and 2100°C.**

**2.5. Porosity overview**

A wide range of porosity and pore size and shapes have been produced by the methods described in previous sections for both $ZrB_2$ and $TiB_2$. In order to put these numbers into perspective, our results of replica, particle stabilized foams and ice templating have been compared with literature values of other porous materials used for a number of applications, including thermal insulation (see Figure 11). It is very encouraging that the porosity achieved in our research so far produced so far are in the correct range for this application.

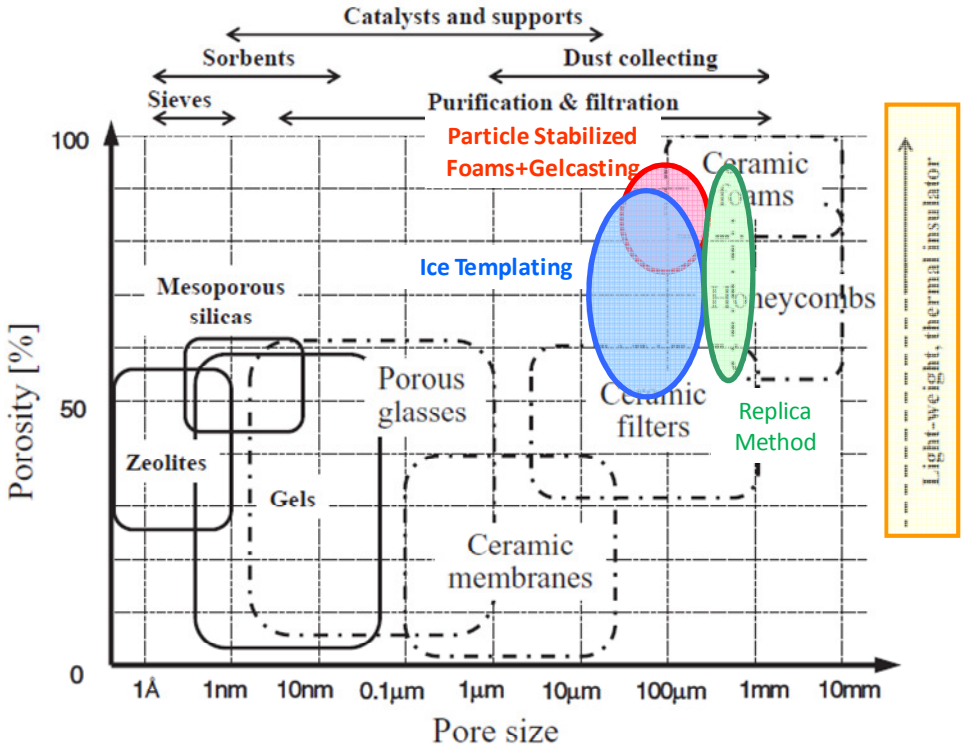


Okada, K., et al. (2011). "Porous ceramics mimicking nature-preparation and properties of microstructures with unidirectionally oriented pores." Science and Technology of Advanced Materials **12(6).**

**Figure 11. Comparison of our porous materials with other materials and applications (15).**

### 3. Near-net-shaping of large complex-pieces

The optimization of the processing conditions have been carried out using small cylindrical (and cubic for replica) samples of 20-22 mm diameter and 20 mm height. One of the requirements for any of these techniques to be useful is to be able to produce full-sized components with the same porous structure and properties as the optimized small samples with no drying cracks.

Large complex pieces in the shape of a rotor and a combustor have been successfully produced by these techniques as shown in the Figures 12 and 13 below. It is important to note that all these shapes are produced as-molded. No polishing or sand-paper has been used to smooth their features before taking these photos. Small roughness and spots can be smoothed before sintering for better finishing. However, no diamond machining is required to shape the materials.


**Figure 12. $ZrB_2$ foams produced by particle stabilized foams and gelcasting. The tapered conical cylinder was chosen to resemble the shape of a combustor.**

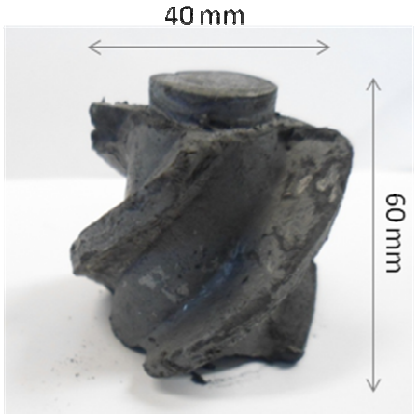


**Figure 13. $ZrB_2$ porous material shaped as a rotor using ice templating.**

These components demonstrate the successful translation of our previous research (6) on producing large complex shaped oxide particle stabilized foams into UHTC materials. Also, our previous work in UHTC for leading edges has demonstrated that it is possible to produce reliable large components of UHTC by combining the colloidal near-net-shaping (as the one used in these images) and pressureless sintering (4).

## 4. Microstructure-Properties Characterization.

After optimizing the processing conditions for each of the routes, samples were characterized using scanning electron microscopy (SEM), density and porosity, X-Ray micro-tomography, thermal conductivity measurements and mechanical testing, in order to establish and understand the relation between their actual microstructure and the desired properties.

Only one condition per route was selected for this stage of the project. The experimental conditions selected for preparing these samples were chosen based on the porosity, ease of handling and porous microstructure found during the optimization stage. Figure 14 shows the microstructure and average porosity of the conditions selected for the characterization.

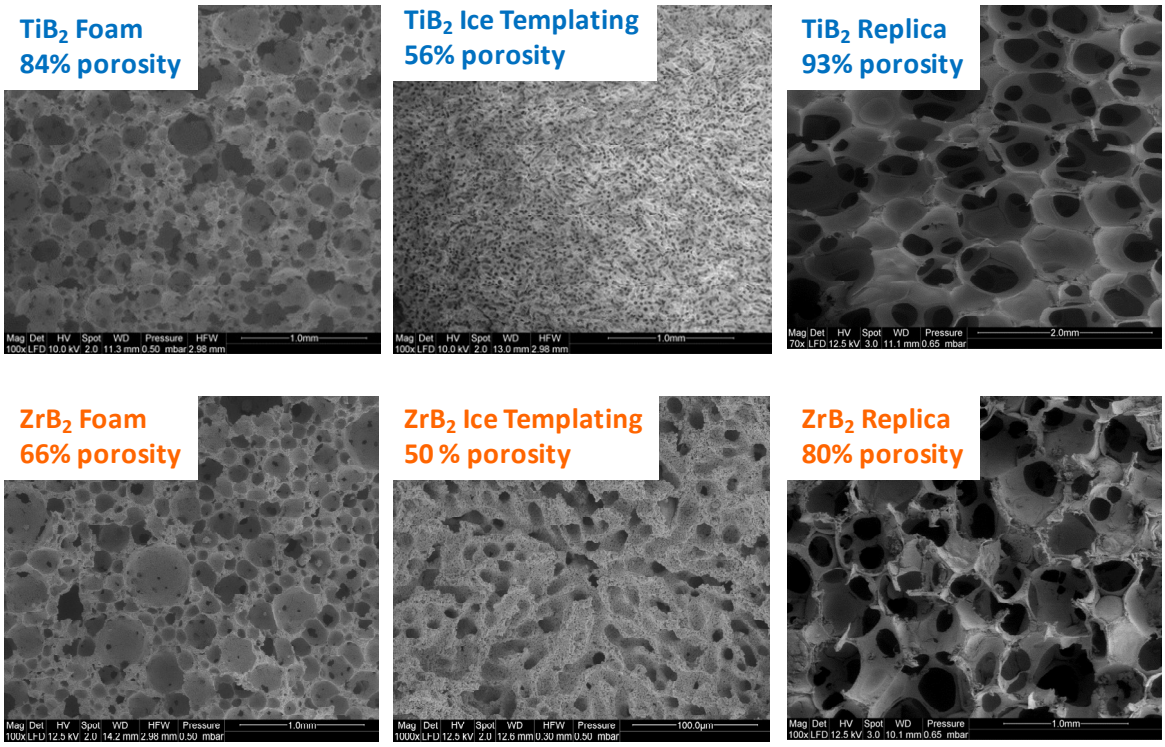


**Figure 14. SEM images of the selected conditions for tomography and thermal and mechanical characterization**

Cylindrical samples for particle stabilized foam and ice templating and cubic samples for replica were prepared with dimensions around 22mm diameter and 25 mm height (equivalent cube length dimensions for replica samples) and were sintered at 2000$^{o}$C/1h. The sintering at this temperature allows the samples to have an additional level of porosity at the micro/nano scale as explained before. The materials produced and to be characterized in the following section have *two-scale porosity*.

*4.1. X-Ray Micro Computed Tomography.*

The objective of this analysis is to have information of the 3D microstructure of each of the material produced, and understand how the porosity changes across the cross section and height of the samples. This technique provides 2D "slice" images across the volume of the sample. These images can be also used to generate a 3D-reconstructed virtual sample for properties modelling, as it will be described in the next section.

The tomography was performed in the Australian National Fabrication Facility-SA Node (Ian Wark Research Institute, University of South Australia). Examples of the images obtained are shown in Figure 15 Due to the limitation in the resolution of the images, some of the smaller porosity cannot be successfully captured, like the micro-sized scale due to the partial sintering.

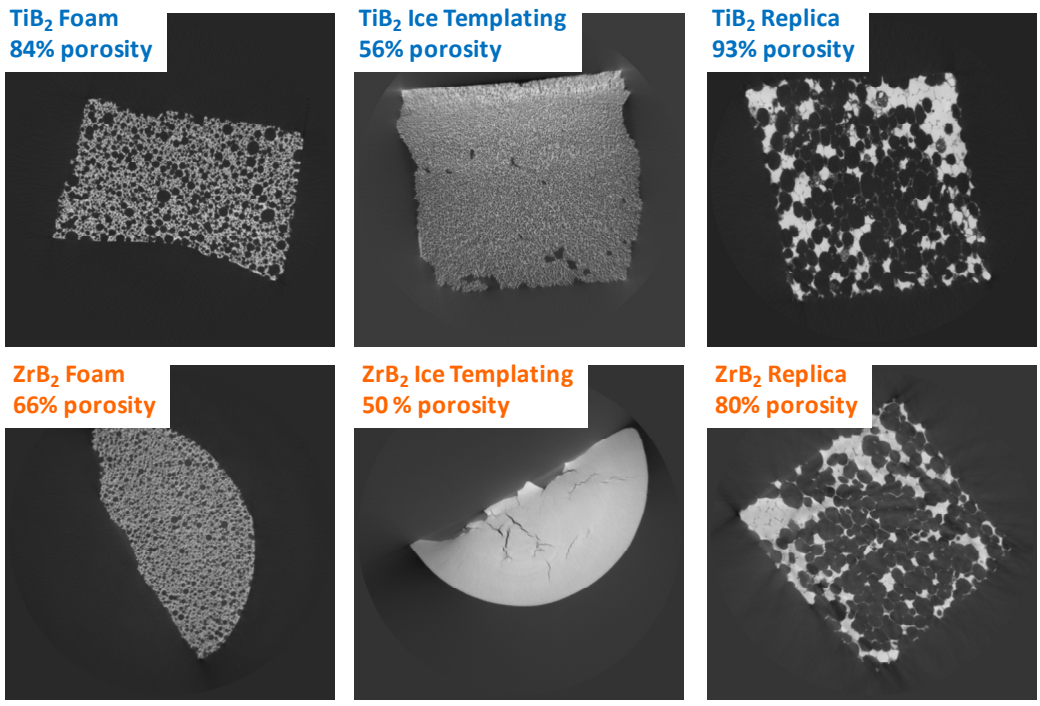


**Figure 15. Examples of x-ray tomography images obtained for the selected materials for the characterization study.**

*4.2. Thermal Conductivity Measurements.*

The thermal conductivity measurements were kindly performed by Dr. Guillermo Narsillio (Department of Infrastructure, The University of Melbourne) using a C-Therm TCi analyser. Three individual samples for each of the selected conditions were analyzed. The thermal conductivity was measured at different points of the different faces of the samples. The results are shown below (Figure 16):

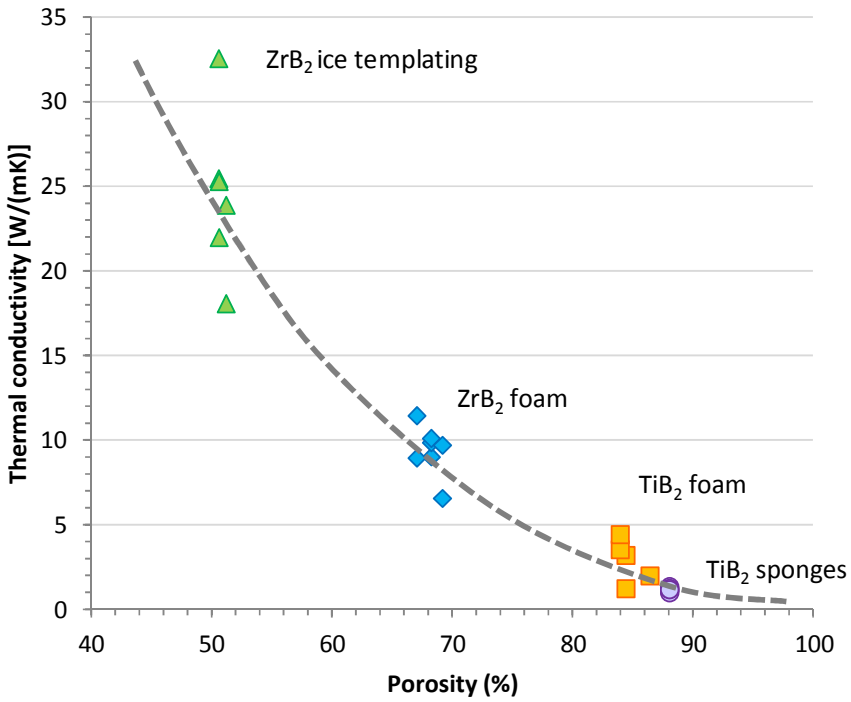


**Figure 16. Thermal conductivity as a function of porosity for the different samples considered for the characterization stage.**

The thermal conductivity decreases with increasing porosity. The porous samples prepared using different techniques have thermal conductivities in a wide range of values, allowing for tailoring of the microstructure depending on the desired application. This trend also is related with the pore size. Samples produced by ice templating at -40°C have in general pore sizes between 20 and 80um, while the foams measured in this experiment have pore sizes between 100 and 300um. The sponges produced by replica have pore sizes between 500 and 1000um. A combined thermal conductivity of around 5 W/mK is generally recommended for aerospace applications[16]. This value of thermal conductivity can be achieved using the materials prepared in this project.

*(Note: the thermal conductivity measurements have been performed as a in-kind contribution to this project. There are two conditions waiting for testing at the time of submission of the present report. The results will be sent on an appendix to this report in the next months).*

### *4.3. Mechanical Testing.*

Despite their potential application as thermal insulation for hypersonic applications, the foams need to withstand certain mechanical loads related with the handling and assembling with other components, in addition to vibrational loads and thermal stresses. All the conditions selected for this study produced samples which can be easily handled in green and sintered stages, and they are able to be lightly machined.

The mechanical testing involved axial and diametral compression on the selected porous materials to determine the compressive and tensile strength, respectively. The elastic modulus was also calculated from the stress-strain curve obtained in the axial compression. Both mechanical testing were performed using an Instron machine, (model 5569A, Canton, Massachusetts) with a load cell of 50 kN (model 2525-802) and compression plates (150 mm diameter, models 2501-084 & 2501-163 (top and bottom, respectively)). The tests were carried out at a loading rate of 0.1 mm/min. An average of 3 samples for each condition was tested in each way. Replica samples were only tested in compression due to their cubic geometry. Examples of the stress-strain curves obtained for the processing routes selected are shown in Figure 17.

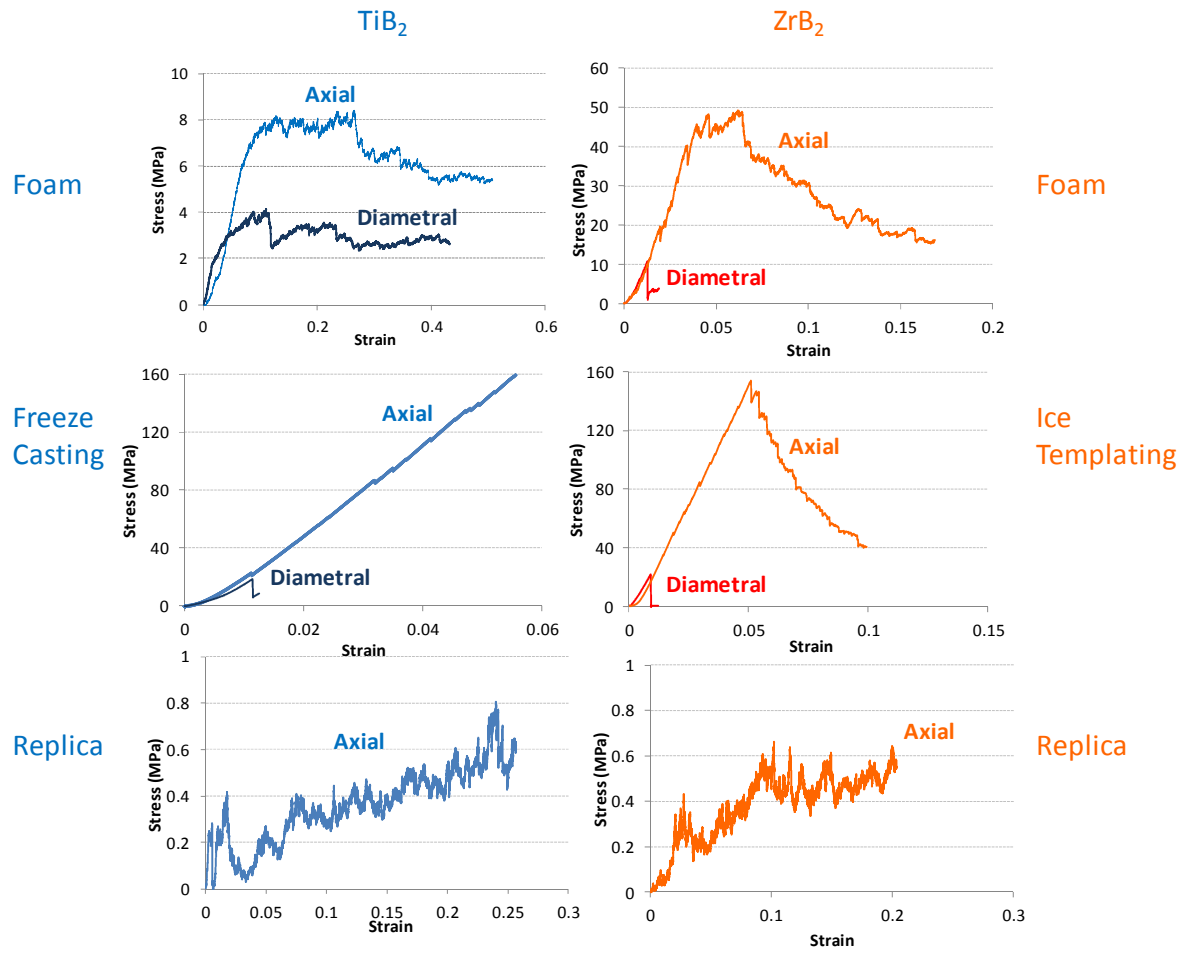


**Figure 17. Stress-strain curves for the selected materials tested under axial and diametral compression. The replica samples were only tested under axial compression due to their geometry.**

In general, the compressive stresses that the different porous samples were able to withstand were much higher than the tensile stresses, as expected for ceramic materials. The ice templating samples showed a more brittle behaviour when compared with the two other type of porous samples. The foams and replica sponges behaved more plastically under the applied load, being able to bear higher deformations before failure (Figure 17). This behaviour is typical in cellular-type ceramics, where the failure of the sample is due to the sequential fracture of the struts[17,18]. The relation between compressive and tensile stresses, elastic modulus and the porosity of the samples are shown in Figure 18. As expected, when the porosity increases, the mechanical strength decreases. There is less "solid" material to bear the load. The maximum compressive and tensile strengths were found for the $ZrB_2$ samples (which also have the lower porosity), being 130 and 20 MPa respectively. Both replica materials showed similar compressive strengths despite being prepared with different materials.

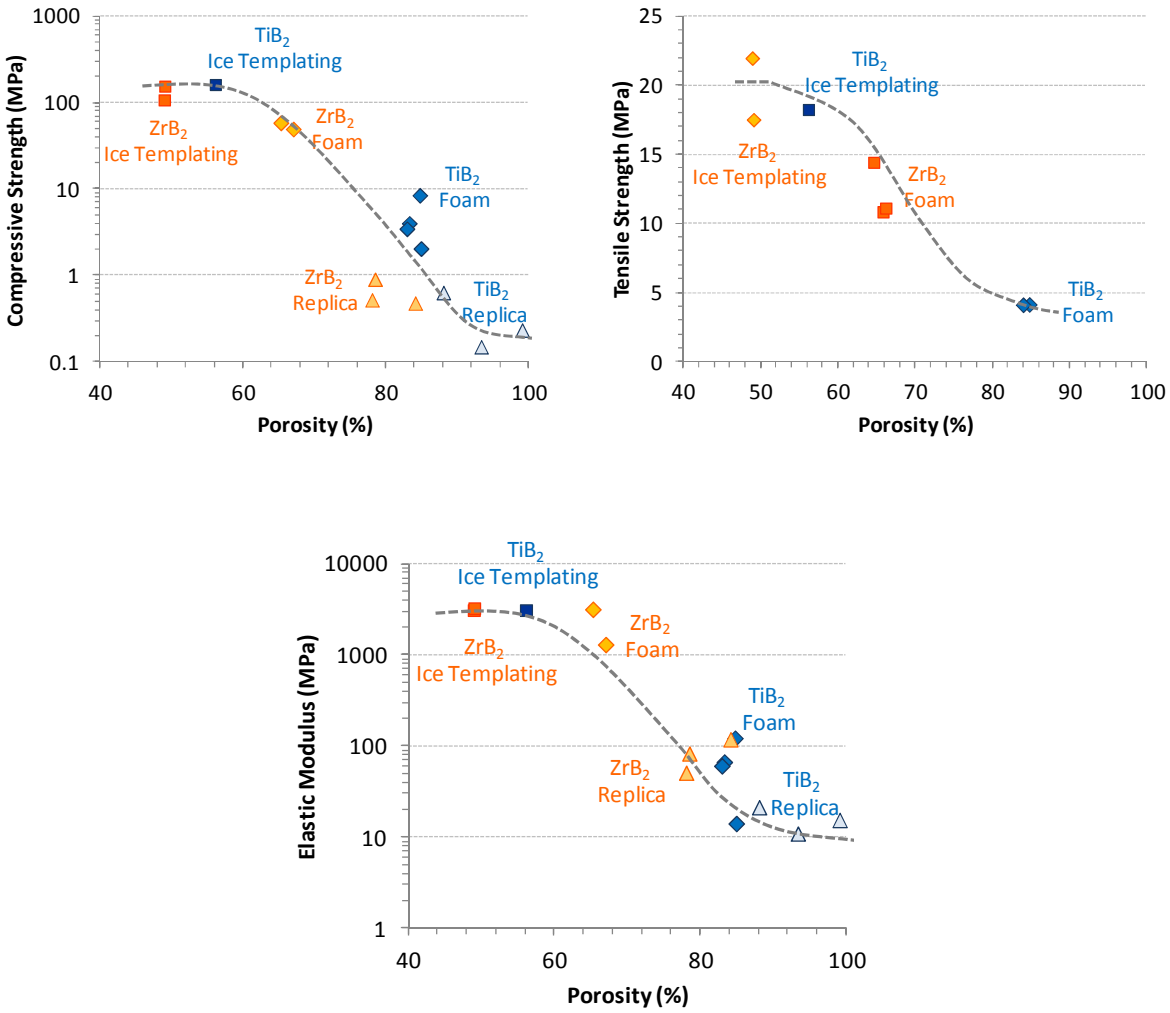


**Figure 18. Compressive and tensile strengths and elastic modulus measured for the samples as a function of the porosity.**

Both ice templating materials had a much higher elastic modulus than the foams and replica materials. The decreasing elastic modulus for higher porosities has been also reported by other authors in similar porous materials[19-21].

## 5. Modelling and Prediction of Porous Ceramic Properties.

The design and optimization of materials relies on their performance under the service conditions. However, relevant testing of materials could be time and cost consuming, and in the case of extreme applications, there are not many testing rigs to replicate the environment and it may not be possible to know the performance of the materials at ultra high temperature, for example. Due to this reason, the characterization of the six chosen materials described in section 4 is used to validate

the thermal and mechanical modelling. The models will be then able to predict their performance under more demanding conditions.

Apart from the experimental data collected for $TiB_2$ and $ZrB_2$ in this project, the modelling of thermal and mechanical performance of porous materials and its relation to their microstructure will also consider an oxide ceramic porous material produced using one of the processing routes described in this report. $ZrO_2$ foams are used as benchmark material for this modelling, due to their wide range of data available in the literature both experimentally and from the modelling point of view.

*5.1. 3D image reconstruction.*

X-ray Micro-Computed Tomography (MCT) was used to capture the microstructure of the porous samples (Figure 15). The result of the MCT is a group of 2D images taken at different planes (slices) throughout the sample. These images need to be processed and stacked back into a 3D reconstructed image to be used for the modeling. The processing of the images was done with the program Fiji (ImageJ Version 1.47b). The main steps and objective of the processing of the images are:

| **Step** | **Objective** |
|---|---|
| - *Image Rotation and Cropping:* | Center and remove unwanted edges and part of images. |
| - *16-bit to 8-bit image conversion:* | Reduce the size of the 2D images |
| - *Contrast adjustment:* | Enhance the difference between solid and pore areas |
| - *Image Sharpening:* | As the previous stage |
| - *Anisotropic Diffusion Filtering:* | Remove graininess and background noise |
| - *Image Segmentation:* | Identify material and pore phases, assigning the right black/white/gray scale to the image. |
| - *Assigning a Physical Extent:* | Relate pixels and size scale of the images |

As an example, Figure19 illustrate the image processing for the $TiB_2$ foam tomography images.

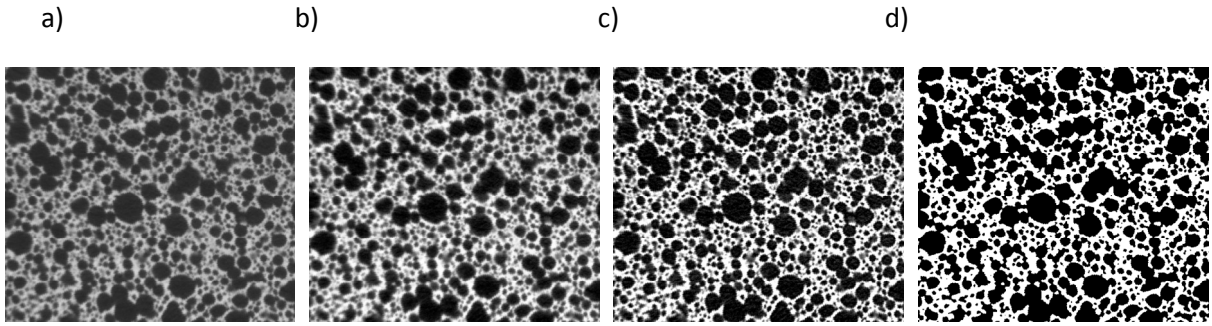


**Figure 19. Example of image processing of $TiB_2$ foam. a) original image, b) after contrast adjustment, c) after the sharpening and d) final segmentation.**

This process is repeated for the selected number of 2D images (from 200 to 1200 slices depending on the resolution and number of pixels of the images). The 2D images are then stacked together to produce a cubic 3D cubic reconstructed image of the actual sample. This is achieved by the voxelization process, in which depth is added to an image by using a set of cross-sectional images, such as the ones produced in the tomography analysis. The tomographic datasets include a "pixel spacing", and a "inter-slice" distance between images. This "inter-slice" distance represents a real-world depth. The 2D images are stacked in computer memory based on interpixel and interslice distances to accurately reflect the real-world sampled volume. The 3D reconstructed images for the materials considered in this section are shown in Figure 20.

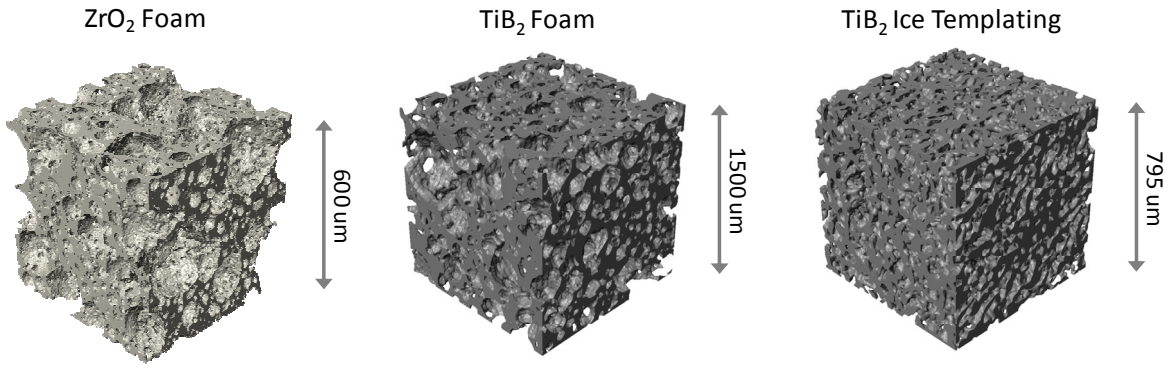


**Figure 20. 3D reconstruction of the microstructure of porous materials considered in this study: $ZrO_2$ foam (reference and benchmark), $TiB_2$ foam and $TiB_2$ ice templating (Freeze Casting).**

*5.2. Creation of the Strut Structure.*

The porous microstructure of each of the considered samples is comprised of a macro porosity corresponding to the processing technique selected but also a micro-scale porosity in the material struts, as a consequence of the particle packing and the partial sintering of the samples (Figure 10). These finer features are not captured by the tomography scanning, since they are below the resolution of the scanner used in this project. However, this micro-scale porosity also plays a significant role in the thermal conductivity and mechanical properties of the porous materials.

In order to consider its contribution to the bulk properties, a modeling technique was used to simulate this level of porosity and to generate a 3D reconstructed image similar to the ones produced from the tomography analysis of actual samples. Using a series of Matlab (version 8.1.0.604 (R2013a)) scripts, spheres were dropped into an enclosed cylindrical domain (Figure 21 a). A cubic section of this domain was then selected (Figure 21b). This 3D section is then converted into a stack of 2D images, representing "slices" throughout the cube (Figure 21). These images will be used as the "starting" point of the 3D image reconstruction, following a similar process as the one described before for the experimental tomography images. The result is a segmented image; where black area represents the pore area of the image and the white area correspond to the solid area in the 2D image (Figure 21c). The 2D images are stacked back together, as described in the previous section. Using a voxel counter program option within Fiji software, the solid and pore volume fractions is calculated. The calculated value is approximately 38%, which is in good agreement with the experimental values for $TiB_2$. However, the "created" microstructure does not resemble very well a partially sintered ceramic material. In order to simulate the "necking" between particles during sintering, a 3D median filter (smoothing) was used twice on the images to produce larger contact area between spheres (Figure 21d). This leads to a decreased in the porosity of this final 3D reconstructed image (Figure 22) to 37% for $TiB_2$. A similar procedure will be done for ZrB2 to create a strut structure with 16% micro-scale porosity.

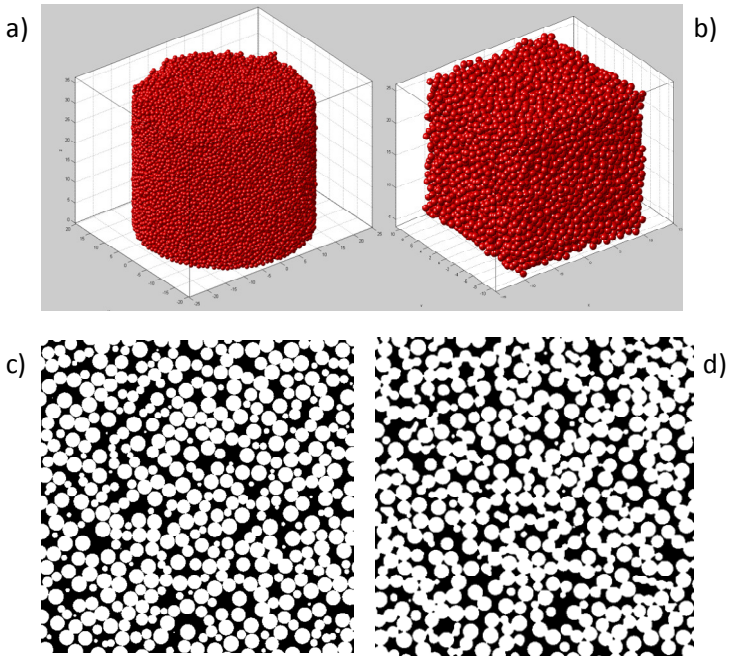


**Figure 21. Illustration of the process of the creation of the porous nanostructure for the thermal and mechanical modelling.**

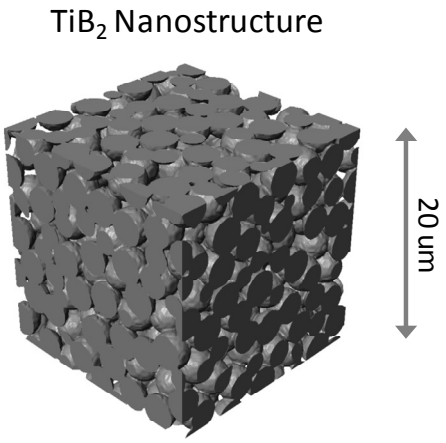


**Figure 22. 3D reconstruction of the porous nanostructure created by random packing of spheres.**

### *5.3. Determination of the Representative Volume Element*

The 3D reconstructed images of the porous materials represent a challenge for the computing simulations, due to their "large" size and data associated. For example, for $TiB_2$ foam the total 3D volume reconstructed is 1500 x1500x1500 um. Therefore, the next step is to determine the minimum volume of that 3D reconstructed image which will accurately predict the porosity, thermal and mechanical properties, while keeping the computation times within reasonable limits (2-3 weeks simulations).

Since they are porous materials, the criteria to follow will be to select a smaller volume within the reconstructed material. In order to do this, several sections (the number of small cubes selected depend on the size selected) within the total cubic 3D reconstructed image were selected. The length scale of these small cubes was chosen to be larger than the average pore size measured in the SEM images. For each of these small cubes, the volume fraction of pore and solid was calculated using a voxel counter program option within Fiji software. The results of porosity for different cubic element sizes are plotted in Figure 23. The variation is much larger for small sizes cubes while the large cubes include a sufficiently large volume to accurately represent the material.

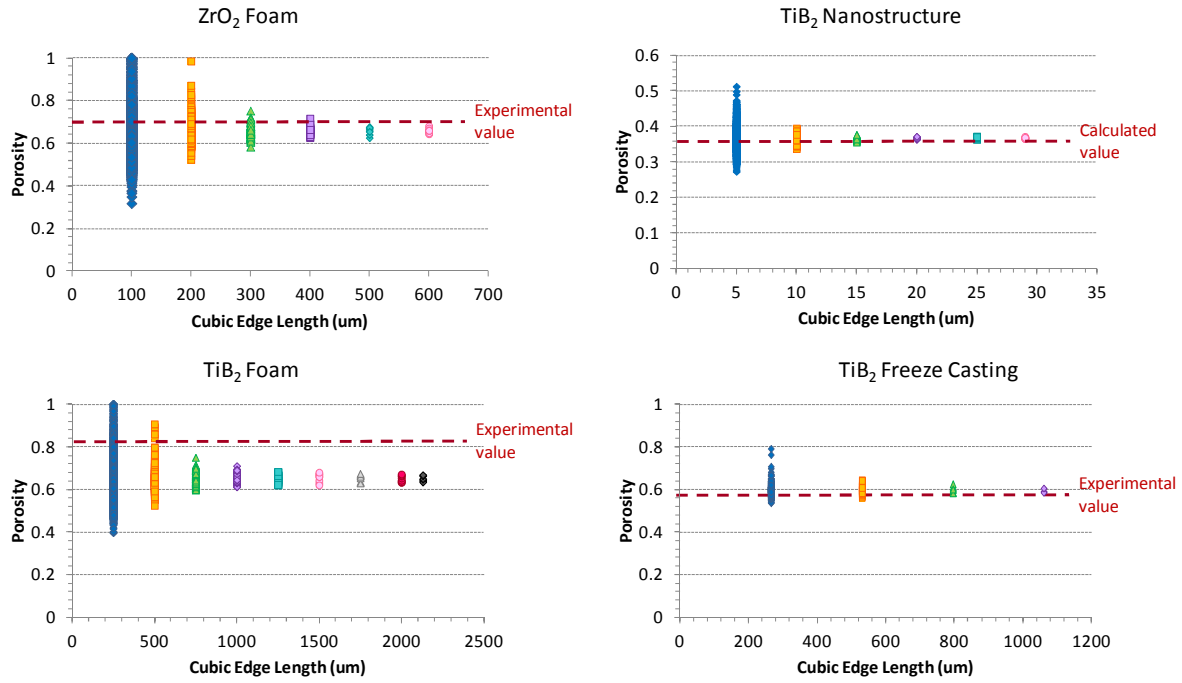


**Figure23. Porosity versus cubic edge length of the cubic elements within the 3D reconstructed material. These plots provide information about the Representative Volume Element (RVE) that will represent the reconstructed material properties for the simulations.**

The average calculated values of porosity for different sections of the 3D reconstructed material are close to the experimental values. The differences between the calculated and the experimental porosities are related with the resolution of the 2D tomography images. These images fail to capture properly some of the smaller porosity features of the sample, and therefore the segmentation process lead to a slight overestimation of the amount of solid in the sample due to difficulty assigning the right black/white/gray scale to those smaller features.

When the size of the element selected is smaller and close to the pore size of the sample, there is a larger scattering between the results of calculated porosity. This indicates that that element size does not properly represent the porous features that characterize a particular sample. It is likely that some of these elements will be mainly solid and other ones, mainly pores. When the size of the selected element increases, the calculated porosity is more similar for all those elements, meaning that any of them will provide a good representation of the microstructure of the material. When the standard deviation of the porosity values is below 5%, it is considered to be a good representation of the microstructure. There are several sizes that match this first part of the criteria. Next, the experience in modeling dictates the maximum size to work with to ensure a reasonable computing simulation time. The selected sizes for each samples are the following (Table 1):

**Table 1. Cubic edge length for the maximum 3D reconstructed cube and for the RVE selected for the thermal and mechanical modelling.**

| Sample | 3D-reconstructed Cubic Edge Length | RVE Cubic Edge Length |
|---|---|---|
| $ZrO_2$ | 13367 um | 600 um |
| Nanostructure | 59 um | 15 um |
| $TiB_2$ Foam | 4261 um | 1750 um |
| $TiB_2$ Ice Templating | 1592 um* | …. |

*Prismatic shape reconstructed: 3182.5 microns x 1591.2 microns x 1060.8 microns

The size which meet both criteria constitute the minimum Representative Volume Element (RVE) and those elements will be used in the thermal and mechanical simulations of the porous materials properties.

(*Note: The 3D reconstruction of the images from x-ray tomography and the determination of the RVE for each reconstructed material is a computing intensive operation. Computing resources were also in used for the actual thermal and mechanical simulations. At the time of submission of this report some materials reconstructions are still in progress. An update of the results will be provided as an appendix to this report in the near future)*

*5.4. Modelling of the Thermal Conductivity of Porous Materials.*

The modelling of the thermal conductivity of the porous materials has been performed using the Lattice Monte Carlo (LMC) Method. Using the RVE determined in each case, a regular, cubic lattice is imposed, and every voxel in that lattice is assigned material properties, in this case thermal conductivity. The thermal conductivity of the ceramic (2.82 W/mK for $ZrO_2$ and 96 W/mK for $TiB_2$)[22,23] is assigned to voxels in the solid and zero thermal conductivity is assigned to the void space (porosity). Discrete thermal energy packets (energy quantums) as defined as particles, which will move throughout the material (jump between lattice sites), creating a "thermal flux" (Figure 24). These particles do not interact with each other, and multiple particles may reside at the same site. The probability of a successful particle jump is proportional to the thermal conductivity difference between the material and the pores (zero).

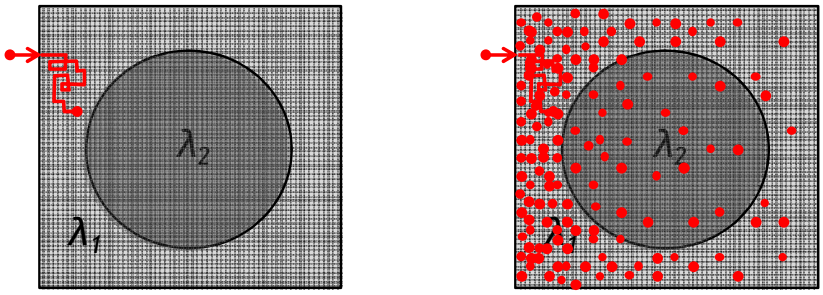


**Figures 24. Illustration of LMC modelling used in this project.**

After a certain time, the distribution of the thermal energy particles will give us the thermal profile across the material. The mean square distance travelled by the particles at the end of the considered time will be used to calculate the effective thermal conductivity. Using the Einstein-Smoluchowski equation for thermal diffusivity,

$$D_{eff} = \frac{< R^2 >}{2dt_{MC}}$$

where $<R^2>$ is the mean square displacement of the heat particles, d is a dimensionality, and $t_{MC}$ is the number of jump attempts, we can derive an effective thermal conductivity (leff) as:

$$\lambda_{eff} = (\rho C_p) D_{eff}$$

where ρ and Cp are the density and calorific capacity of the material, respectively. Cp is temperature dependant. The initial simulations have been done at room temperature. An average of $10^7$ heat particles and $10^6$ steps have been used for most of the simulations in this report. (A detailed study of the influence of these two parameters in the simulation is not shown here).

The thermal simulation using LMC algorithm on an already data-intense-3D reconstructed microstructure is very demanding in terms of resources and runtime to complete the simulation. In order to achieve a good simulation and manage the immense amount of data implemented and produced, this modeling was performed using parallel computing on a GPU (Graphics Processing Unit, run on HP Z800 computer, with a CPU Intel Xeon X5660 @ 2.8GHz 24 GB memory and GPU: Nvidia Tesla K20c). The reduction in runtime is remarkable when compare with a single core computer, as illustrated in Figure 25.

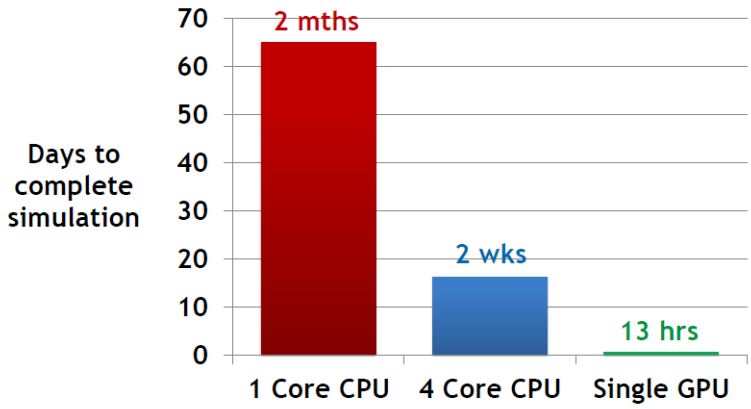


**Figure 25. Comparison of runtime of LMC simulations on 1 and 4 core CPU versus a single GPU. (M. Wang, PhD thesis, The University of Melbourne).**

For a 66% porosity $ZrO_2$ foam, the predicted value of thermal conductivity is 0.37 W/mK. The average experimental value is 0.45 W/mK, showing a good agreement between experiments and predictive modeling.

As described before, in the case of $TiB_2$ porous materials, it is necessary to consider the micro-scale porosity in the struts. Separated simulations were carried out using the LMC-GPU modeling technique on the created strut structure and on the 3D reconstructed microstructures from the experimental tomography data. The combined results of the simulations are shown below in Table 2.

**Table 2. Simulated and Experimental values for thermal conductivity**

| Sample | RVE calculated Porosity (%) | $\lambda_{LMC}$ (W/m K) | $\lambda_{EXP}$ (W/m K) |
|---|---|---|---|
| $ZrO_2$ foam | 66% | 0.37 | 0.45 |
| $TiB_2$ Nanostructure | 37% | 32.3 | In progress |
| $TiB_2$ Foam | 78%^ | 5.6 | 2.85 |
| $TiB_2$ Ice Templating | 75%^ | 5.6 | In progress |

*^ including the porosity of the nanostructure.*

These data are in very good agreement with the experimental values, as described in the previous section 4.2. validating the suitability of the modeling approach used to predict thermal conductivity of porous materials.

*5.5. Modelling of the Mechanical Properties.*

The modelling of the mechanical properties of porous materials has been attempted using Finite Element Analysis (FEA) approach. The mesh for the FEA was created using Simpleware (Version 6.0) while the mechanical simulations were performed in Abaqus (Version 6.12-AP) (run on a computer HP Z800, with a CPU Intel Xeon X5660 @ 2.8GHz, 48GB memory and GPU Nvidia Quadro 5000).

In this modelling approach, the RVE of the 3D reconstructed image is meshed (using the +FE Free algorithm in Simpleware, that create a tetrahedral mesh that conforms to the features of the segmented image). The meshing elements are responsible to provide the correct node location and elastic properties to capture properly the response of the material under an applied load (Figure 26).

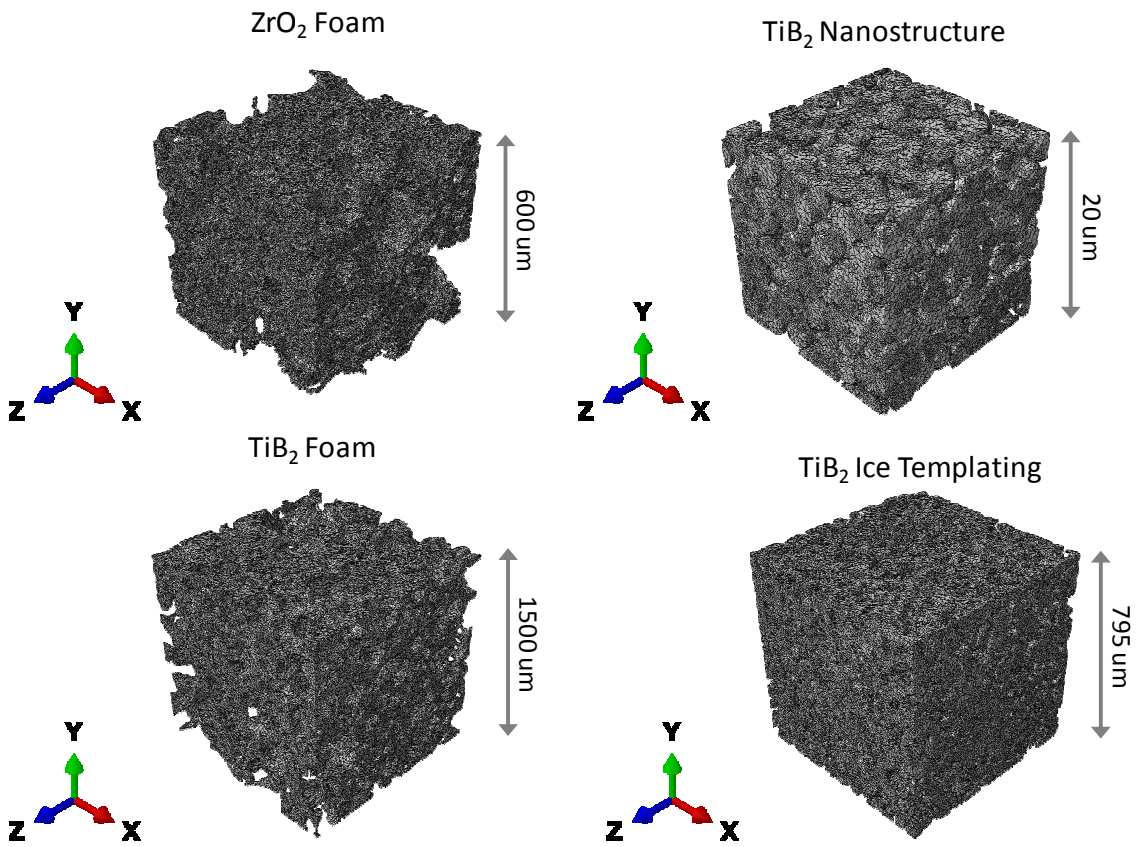


**Figure 26. Meshed elements for FEA modelling of mechanical properties corresponding to the porous materials considered in this report.**

Each element of the mesh will be allocated a set of values from the bulk materials. In this, case, each element is allocated a value of elastic modulus (187 GPa for $ZrO_2$ and 565 GPa for $TiB_2$)[24,25]. The load will be applied on the 3 main directions (x, y, z) on the meshed RVE. The load is uniformly applied all over the selected X/Y/Z surface, as shown in Figure 27. In this case, the load was applied by defining a given displacement (strain) upon that surface.

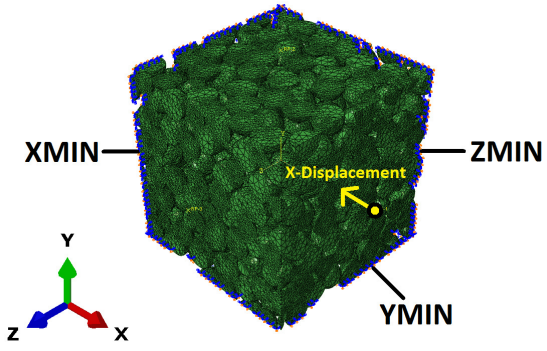


**Figure 27. Example of displacement applied in the x-direction for the $TiB_2$ nanostructure.**

A simple linear-elastic model was selected for the initial simulations. This model assumes that the material and structural stiffness are constant and that they cannot change during the analysis. Any changes in stiffness due to material changes (plasticity or fracture), geometry (e.g. buckling of the struts) or contact (e.g. between struts) have not been factored into the simulation. The stress contour maps for the different samples considered in this study when a uniform displacement is applied in the X-direction are shown in Figure 28. In these stress contour maps, the displacement (strain) applied are 1% for the $ZrO_2$ Foam and $TiB_2$ nanostructure, and 0.1% for the $TiB_2$ Foam and $TiB_2$ ice Templating. Similar stress contours were found when applying the strain in the y and z direction.

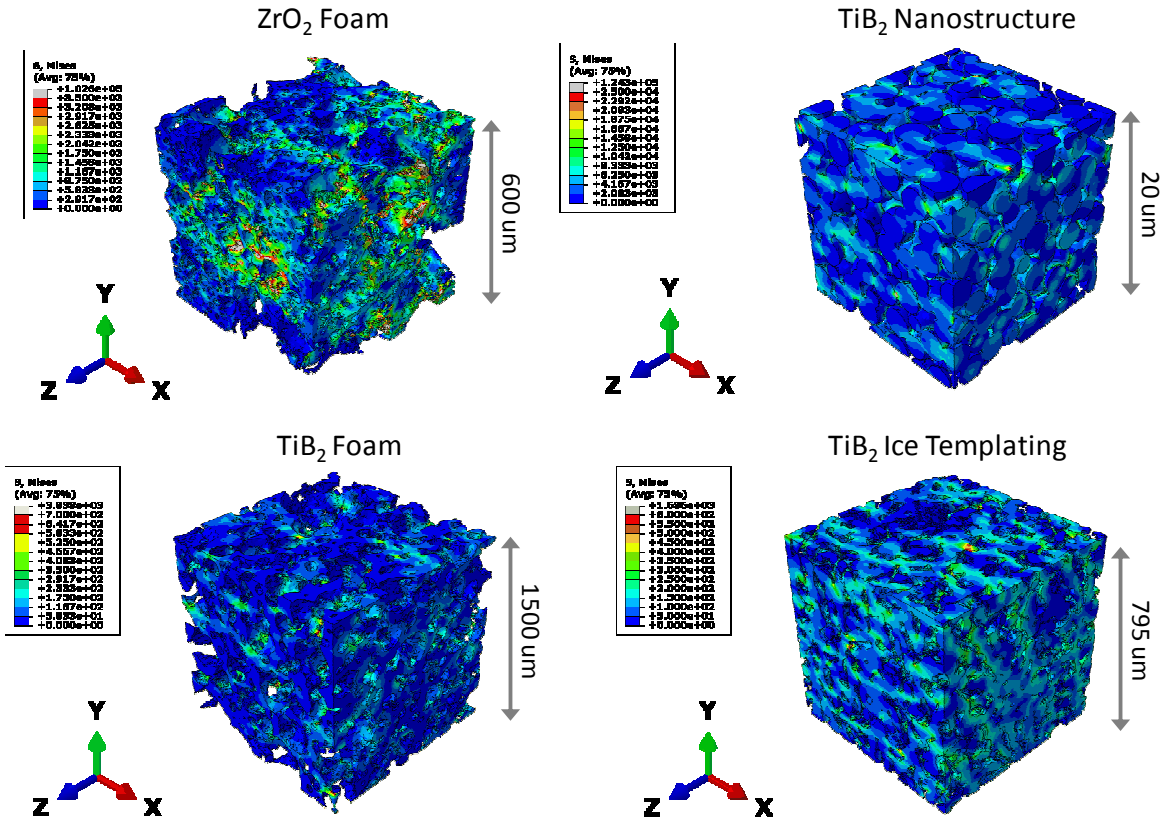


**Figure 28. Stress contour maps for the materials selected for this study when a displacement is applied in the x-direction. The stress contours are shown are in MPa.**

For each direction, a value of stress and elastic modulus can be calculated for each material. As an example, Figure 29 shows the stress-strain curve for the 3 directions for the reference $ZrO_2$ sample. Since this simulation was done using the RVE for this material, there are not significant differences between the mechanical behavior predicted in x, y and z. For volumes less than the RVE, there is a higher scatter in the values for stresses and elastic modulus in the 3 directions.

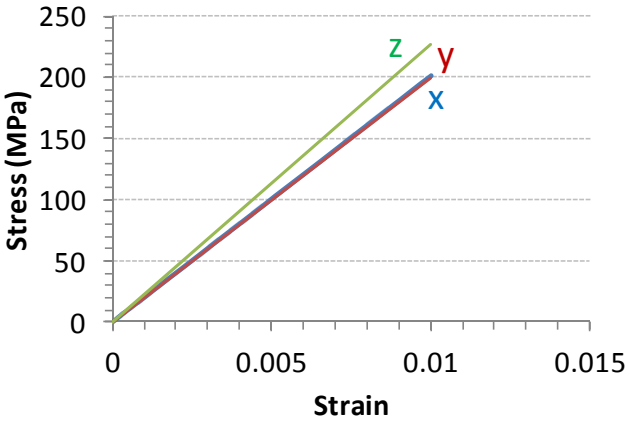


**Figure 29. Stress-strain curve in the x,y and z direction for the reference $ZrO_2$ sample.**

This stress-strain curves are quite different from the experimental ones. The average stresses and elastic modulus predicted by this linear-elastic model in the x, y and z directions are summarized in Table 3:

**Table 3. Simulated mechanical values for the samples used in this study.**

| Sample | Porosity* (%) | RVE length (um) | Strain (%) | Compressive Stress (MPa) (average x,y, z) | Elastic Modulus (GPa) (average x,y,z) |
|---|---|---|---|---|---|
| $ZrO_2$ Foam | 66% | 600 | 1 | 209 ± 15 | 20.9 ± 1.5 |
| $TiB_2$ Nanostructure | 37 | 20 | 1 | 1766 ± 113 | 176 ± 11 |
| $TiB_2$ Foam | 65 | 1500 | 0.1 | 26 ± 2 | 26 ± 2 |
| $TiB_2$ Ice Templating | 60 | 795 | 0.1 | 69 ± 8 | 69 ± 8 |

*calculated porosity of the RVE reconstructed microstructure.

**Table 4. Experimental mechanical values for the samples used in this study.**

| Sample | Porosity (%) | Compressive Stress (MPa) | Elastic Modulus (gPa) |
|---|---|---|---|
| $ZrO_2$ Foam | 66 | 36 | 1.2 |
| $TiB_2$ Foam | 84 | 4.5 | 0.07 |
| $TiB_2$ Ice Templating | 56 | 161 | 3 |

.

The predicted results are significantly higher than the experimental values (Table 4) for all the porous materials considered to date. This relatively simplistic model fails to capture the elastic behavior of the porous materials prior to fracture. Further optimization need to be performed to

incorporate other factors such as the buckling and fracture of the struts and to incorporate the nanostructure into the model.

In order to improve the modelling approach, the optimization of the element used for the mesh was considered. For this type of linear-elastic simulations a linear element (C3D4) are recommended. However, these elements could be very rigid for such complaints materials as the ones produced in this project. A quadratic element (C3D10) element was also tested. However, this entails larger memory usage, so an initial study was performed on a smaller section of the $ZrO_2$ foam (below the RVE) to compare the usage of these two elements. Figure 30 shows the elastic modulus for both type of elements in the three axis directions. Although the second order elements systematically showing lower values for elastic modulus in the 3 axis, as expected and desired, there are no larger differences respect to the linear elements. In addition, just for the smaller section the simulation took longer than 10 days, which make it impractical for the actual RVE to study.

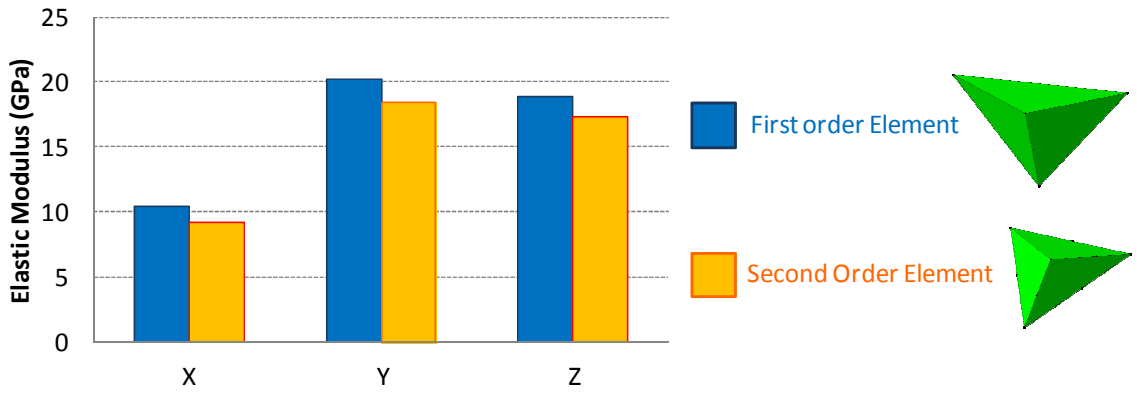


**Figure 30. Elastic modulus simulated for the x, y and z direction for the reference $ZrO_2$ sample using first order and second order element in the FEA meshing.**

## 6. Preparation of Multi-scale Porous Materials

The processing parameters for each processing route were optimized and the most promising formulations have been characterized in terms of tomography, thermal conductivity and mechanical properties. Each of the characterized samples so far contained *two levels of porosity*: macro porosity resultant from the selected processing route and a micro-scale porosity resultant from the partial sintering of the particles in the struts.

From the study of the processing and characterization of the porous materials produced by the different routes, it can be seen that porosity level and pore size similar to those produced by the replica method and partial sintering are the most desirable from the insulation point of view; however, their mechanical strength is really low. A combination of that type of porosity with other processing methods such as the foam, or preferable with freeze casting, will be desirable to boost their mechanical strength.

In order to create the *multi-scale porous materials*, combinations of two processing routes were explored for both materials. Some steps of the experimental procedure were slightly modified to allow the combination of the different routes into a single material. Some of the most successful combinations are shown in Figure 31. Each of those combinations present *three type of porosity* in the same material.

The porosity of these materials ranged from 60 to 90%, depending on the material and combination employed. For example, $ZrB_2$ samples prepared using the 3 processing routes (foam+replica+ice templating) and partial sintering was mechanically tested under axial and diametral compression. These samples exhibit average tensile and compressive strengths of 1.7 and 10MPa approximately, for an average porosity of 62%. Further characterization of the multi-scale materials is intended to continue after the life of this project.

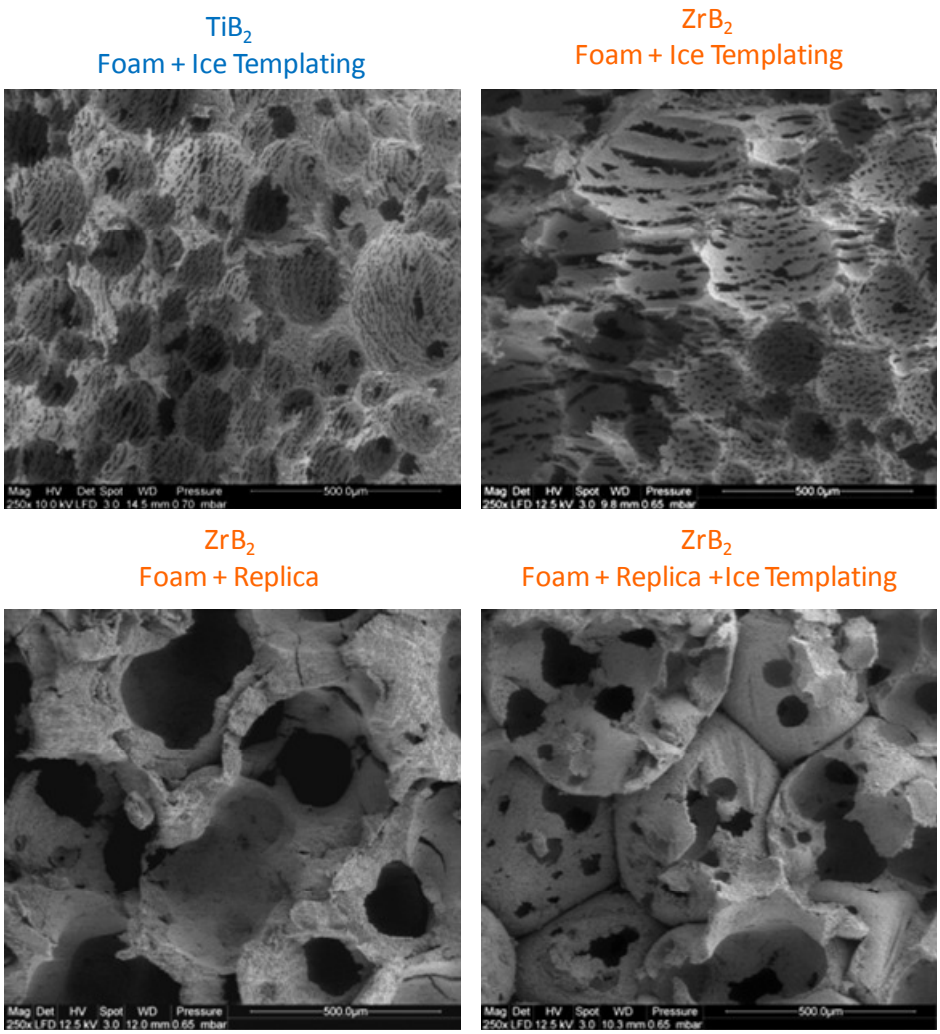


**Figure 31. SEM images of some examples of multi-scale materials prepared combining the processing routes investigated in this work: replica, foam and ice templating. All these combinations also contain the nano/micro porosity level from the partial sintering.**

## 7. Summary

Porous $ZrB_2$ and $TiB_2$ materials have been produced using four different techniques: replica, particle stabilized foams, ice templating and partial sintering. High porosities (up to 92%) have been achieved in both materials. The pore shape and size depends on the processing conditions. The pore size ranges between 20 and 500um. The morphology of the pores can be closed bubble-like porosity, interconnected open porosity and/or lamellar structures. The study of the effect of the main processing parameters of these routes has led to a better understanding of the surface characteristics of both materials. This knowledge is important to ensure that the microstructures prepared in $ZrB_2$ and $TiB_2$ can be reproduced in any desired combination of UHTC materials in the future. These colloidal processing techniques have enabled the preparation of large complex-shaped porous materials. The first steps into the production of multi-scale porous materials has been taken,

yielding porosities between 65 and 90% and microstructures that show the characteristic features of the combined processing techniques. The thermal conductivity and mechanical properties showed a very strong dependence with porosity, showing maximum values for lower porosities materials (i.e. ice templating samples). The x-ray tomography characterization of the tested samples was used to produce a 3D-reconstruction of the microstructure needed for the modelling of the materials properties. Thermal modelling using Lattice Monte Carlo simulation showed a very good agreement with the experimental results. The mechanical modelling using Finite Element Analysis (FEA) using a linear-elastic model significantly overestimates the elastic properties of the porous materials. Further optimization of the FEA model is needed.

## 8. Future work.

Although the project has ended, we will finish the thermal and mechanical modelling of the remaining tomography images for the $ZrB_2$ and $TiB_2$ samples. Further refinements of the FEA model is needed to more accurately model the mechanical properties.

In the long term, this project has provided scientific evidence of chemical differences between the powder surfaces which affects the processing. A detailed study to characterize the surface behaviour and calculate Hamaker constants, attraction and repulsion forces would lead to significant advance in the processing field, not only in the porous area, but on the preparation of dense UHTC for other extreme applications.

## 9. Outcomes and relevance of this project.

The relevance and outcomes at the end of this project are the following:

a) Development of multi-scale porous UHTC materials with the ability to produce large complex shapes as well as controllable amount, size and morphology of porosity. The low density material is expected to have low thermal conductivity and good strength. This will enable the design of thermal protection systems for applications such as leading edges and combustors operating in hypersonic conditions.

b) Improved understanding of the role microstructure plays on properties of porous materials at extreme conditions: Heat conduction through the structure as a function of total porosity, pore size and shape.

c) Prediction of the performance of these materials as insulation elements in aerospace applications under severe thermal loads. The predictive modelling will allow tailoring the porous microstructure to optimize performance in specific applications.

d) Improved fundamental knowledge and understanding of the role surface chemistry plays on colloidal processing of UHTCs. This will help the UHTC community to enhance the understanding of not only the preparation of suspensions for shaping but also the densification behaviour of UHTCs.

## 10. Publications

### a) Contribution to conferences

Part of the work developed within this project has been included in the following presentations to conferences:

- "Multi-Scale Porous Ceramics: Microstructure-Properties Modelling", G.V. Franks, C. Tallon, P.J. Mignone and M. Wang, 3rd Biennial Conference of the Combined Australian Materials Societies, 26-28 November 2014, Sydney (Australia).
- "Multi-Scale Porous Ceramics: Near-Net-Shaping and Processing", C. Tallon and G.V. Franks, 3rd Biennial Conference of the Combined Australian Materials Societies, 26-28 November 2014, Sydney (Australia).
- "Control of the Microstructure of Porous Ceramic Materials", Invited talk, C. Tallon for G.V. Franks, *12th International Conference on Ceramic Processing Science*, 4-7th August 2013, Portland, Oregon (US).
- "The Role of Interparticle Forces in the Preparation of Non-Oxide Ceramic Dense Materials and High Porosity Foams", C. Tallon and G.V. Franks, *Australia-Japan Colloid Surface and Science Symposium*, 18-20th September 2013, Nagoya (Japan).
- "Challenges in the Preparation of Borides and Carbides Powder Concentrated Suspensions for Near-Net-Shaping of UHTC Ceramics", C. Tallon, S. Leo, C. Minas and G.V. Franks, *6th Pacific Rim Conference on Rheology*, 20-25 July 2014,The University of Melbourne, VIC (Australia).

**b) Publications**

We are preparing the following manuscripts at the moment to be submitted to the highest impact factor SCI journals in the ceramic processing field:

- Highly Porous Zirconia Materials: Processing and Modelling", C. Tallon, M. Wang, P.J. Mignone and G.V. Franks, to be submitted to J*. Am. Ceram. Soc*., 2015.
- "High Porosity Near-Net-Shaped Titanium Diboride Materials", C. Minas, **C. Tallon** and **G.V. Franks**, in preparation, to be submitted to *J. Eur. Ceram. Soc.* 2015.
- "Multi-Scale Porosity $ZrB_2$ Materials for High Temperature Insulation", **C. Tallon**, L. Jukes and **G.V. Franks**, in preparation, to be submitted to *J. Am. Ceram. Soc*., 2015.

*Additional papers about modelling/tomography collaboration are expected to be prepared towards the end of the project*

The research in this project has also been reflected in the master thesis of Clara Minas, (Visiting master student from ETH Zurich). The title of her master thesis is "Highly Porous Foams from Titanium Diboride Suspensions', submitted to ETH Zurich on 31$^{st}$ Oct. 2013.

## 11. Interaction with AOARD-US Air Force.

C. Tallon was granted a grant from the WOS program to attend the ***Thermal Portfoli Review***, hosted by Dr. Ali Sayir, Dr. Bin-Salamon, Dr. Marshall and Dr. Luginsland, and the ***Aerospace Materials for Extreme Environments Program Review***, hosted by Dr. Ali Sayir, both in Arlington Virginia during May 2014.

The work performed during our first year of the project was presented in the *Aerospace Materials for Extreme Environments Program Review* review with the title "Near-Net-Shaping of Multi-Scale Porous UHTC".

The attendance to these reviews was very beneficial for this project, due to the interaction and discussion with other members of the AFOSR/AFRL/AOARD community. Potential collaborations for the future were also discussed, in particular in the area of modelling-properties prediction. We are planning to pursue some of these initial contacts and discussion points in the near future.

**Acknowledgements**

We would like to gratefully acknowledge AOARD for the funding to develop this work. We also would like to sincerely acknowledge our project manager, Dr. Ken Caster, for his support, help, encouragement and useful discussions before and during this project.

We thank Ms. Clara Minas and Mrs. Laura Jukes for their help with the experiments with $TiB_2$ and $ZrB_2$, and Mr. Paul Mignone for his contribution to this project with the properties modelling.

We would like to acknowledge, Mr. Chris Bassell and Dr. Simon Doe (ANFF, Ian Wark, University of South Australia), Dr. Guillermo Narsillo (Department of Infraestructure Engineering, The University of Melbourne), Mr. Steve Adams (School of Engineering, The University of Melbourne) for their help with the tomography, thermal conductivity and mechanical testing respectively.

Finally we would like to thank the University of Melbourne for infrastructure support and the Defence Materials Technology Centre (DMTC ) for providing the framework to develop this idea and salary support for Dr. Carolina Tallon.

**References**

1. **C. Tallon**, S. Slater, A. Gillen, C. Wood and J. Turner, "Ceramic Materials for Hypersonic Applications", *Materials Australia Magazine*, July 2011, 28-32, (2011)

2. D. E. Glass. "Physical Challenges and Limitations Confronting the Use of UHTCs on Hypersonic Vehicles" in *17th AIAA Space Planes and Hypersonic Systems and Technology Conference*, San Francisco, California, (2011).

3. **C. Tallon** and **G. V. Franks**, "Recent Trends in Shape Forming from Colloidal Processing: A Review", *J. Ceramic Soc. Japan*, 119 [3], 147-160 (2011).

4. **C. Tallon**, D. Chavara, A. Gillen, D. Riley, L. Edwards, S. Moricca and **G. V. Franks,** "Colloidal Processing of Zirconium Diboride Ultra-high Temperature Ceramics", *J. Am. Ceram. Soc.*, 96 [8], 2374-2381, (2013).

5. C. Chuanuwatanakul**, C. Tallon**, D. E. Dunstan and **G. V. Franks**, "Controlling the Microstructure of Ceramic Particle Stabilized Foams: Influence of Contact Angle and Particle Aggregation", *Soft Matter*, 7, 11464-11474 (2011).

6. C. Chuanuwatanakul, **C. Tallon**, D. E. Dunstan and **G. V. Franks**, "Producing large complex-shaped ceramic particle stabilized foams", *J. Am. Ceram. Soc.*, 96 [5], 1407-1413, (2013).

7. T. Ohji, M. Fukushima, "Macro-porous ceramics: processing and properties"**,** *International Materials Reviews*, **2012**, *57*, 115.

8. A. R. Studart, U. T. Gonzenbach, E. Tervoort and L. J. Gauckler, "Processing routes to macroporous ceramics: A review", *J. Am. Ceram. Soc.*, **2006**, 89, 1771-1789..

9. U. T. Gonzenbach, A. R. Studart, E. Tervoort and L. J. Gauckler, "Stabilization of Foams with Inorganic Colloidal Particles", *Langmuir*, **2006**, *22*, 10983-10988.

10. U. T. Gonzenbach, A. R. Studart, E. Tervoort and L. J. Gauckler," Macroporous Ceramics from Particle-Stabilized Wet Foams", *J. Am. Ceram. Soc.*, **2007**, *90*, 16.

11. U. T. Gonzenbach, A. R. Studart, E. Tervoort and L. J. Gauckler, "Tailoring the Microstructure of Particle-Stabilized Wet Foams" *Langmuir*, **2007**, *23*, 1025-1032.

12. U. T. Gonzenbach, A. R. Studart, D. Steinlin, E. Tervoort and L. J. Gauckler, "Processing of Particle-Stabilized Wet Foams Into Porous Ceramics", *J. Am. Ceram. Soc.*, **2007**, *90*, 3407-3414.

13. F. Chabert, D. E. Dunstan and **G. V. Franks**, "Cross-linked polyvinyl alcohol (PVA) as a binder for gelcasting and green machining", *J. Am. Ceram. Soc.*, 91 [10] 3138-3146 (2008).

14. **C. Tallon**, R. Moreno and M.I. Nieto, "Shaping of Porous Alumina Bodies by Freeze-Casting", Adv. Appl. Ceram., 108 [5] 307-313 (2009).

15. K. Okada, T. Isobe, K. Katsumata, Y. Kameshima, A. Nakajima and K. J. D. MacKenzie, "Porous ceramics mimicking nature-preparation and properties of microstructures with unidirectionally oriented pores" Science and Technology of Advanced Materials, 12 (6), 064701, 2011.

16. S. Zhang and D. Zhao, "Aerospace Materials Handbook", CRC Press, 2012.

17. C.Q. Dam, R. Brezny and D.J. Green, “Compressive Behavior and Deformation-Mode Map of an Open Cell Alumina”, J. Mater. Res., [5], 1, 1990

18. P. Colombo and E. Bernardo, “Macro- and micro-cellular porous ceramics from preceramic polymers*”.* Composites Science and Technology, 2003. 63, 2353–2359.

19. S. Dhara and P. Bhargava, “Influence of Slurry Characteristics on Porosity and Mechanical Properties of Alumina Foams*”,* Inter. J. App. Ceram. Technol., 2006. **3**(5): p. 382–392;

20. L. Montanaro, Y. Jorand, G. Fantozzi, and A. Negro, “Ceramic Foams by Powder Processing”,J. Eur. Ceram. Soc., 1998. **18**: p. 1339-1350.

21. P. Colombo, J.R. Hellmann and D.L. Shelleman, “Mechanical Properties of Silicon Oxycarbide Ceramic Foams”, *J. Am. Ceram. Soc.,* **84** [10] 2245–51 (2001).

22. B.-Y. Jang and H. Matsubara. "Thermophysical properties of EB-PVD coatings and sintered ceramics of 4mol% Y2O3 stabilized zirconia." J. Alloys Comp, [419] (1) (2006), 243-246

23. NIST, [ 105], pp. 709-720 (2000).

24. R.C. Bradt, D. Munz, M. Sakai, V.Ya. Shevchenko, K.W. White, “Fracture Mechanics of Ceramics: Crack-Microstructure Interaction: R-Curve” Springer Science & Business Media, 28 Feb 2002.

25. R.G. Munro, "Material Properties of Titanium Diboride." Journal of Research of the National Institute of Standards and Technology 105.5 (2000): 709-720.